Clonal evolution in serially passaged *Cryptococcus neoformans* x *deneoformans* hybrids reveals a heterogenous landscape of genomic change

Lucas A. Michelotti*,[1]

Sheng Sun†

Joseph Heitman†

Timothy Y. James*

*Department of Ecology and Evolutionary Biology

University of Michigan

Ann Arbor, MI 48109 U.S.A.

†Departments of Molecular Genetics and Microbiology, Medicine, and Pharmacology and Cancer Biology

Duke University Medical Center

Durham, NC 27710 U.S.A.

[1]Current address:

Department of Entomology

University of Georgia

Athens, GA 30606 U.S.A.

Raw sequence data has been deposited into NCBI's SRA archive under BioProject: PRJNA700784, with the accession numbers SRX10055646-SRX10055684.

Running title: Lab evolution of hybrid yeast

Key words: polyploid hybrid, trisomic, experimental evolution, evolve and resequence, *Galleria mellonella*

Correspondence:

Timothy Y. James

1105 N. University

4050 Biological Sciences Bldg.

University of Michigan

Ann Arbor, MI 48109 U.S.A.

Email: tyjames@umich.edu

Abstract

Cryptococcus neoformans x *deneoformans* hybrids (also known as serotype AD hybrids) are basidiomycete yeasts that are common in a clinical setting. Like many hybrids, the AD hybrids are largely locked at the F1 stage and are mostly unable to undergo normal meiotic reproduction. However, these F1 hybrids, which display a high (~10%) sequence divergence are known to genetically diversify through mitotic recombination and aneuploidy, and this diversification may be adaptive. In this study, we evolved a single AD hybrid genotype in six diverse environments by serial passaging and then used genome resequencing of evolved clones to determine evolutionary mechanisms of adaptation. The evolved clones generally increased fitness after passaging, accompanied by an average of 3.3 point mutations, 2.9 loss of heterozygosity (LOH) events, and 0.7 trisomic chromosomes per clone. LOH occurred through nondisjunction of chromosomes, crossing over consistent with break-induced replication, and gene conversion, in that order of prevalence. The breakpoints of these recombination events were significantly associated with regions of the genome with lower sequence divergence between the parents and clustered in subtelomeric regions, notably in regions that had undergone introgression between the two parental species. Parallel evolution was observed, particularly through repeated homozygosity via nondisjunction, yet there was little evidence of environment-specific parallel change for either LOH, aneuploidy, or mutations. These data show that AD hybrids have both a remarkable genomic plasticity and yet are challenged in the ability to recombine through sequence divergence and chromosomal rearrangements, a scenario likely limiting the precision of adaptive evolution to novel environments.

Introduction

Hybridization reunites genomes that diverged via speciation. Following speciation, genomes from divergent populations have fixed nucleotide differences as well as usually larger-scale genomic changes such as chromosome rearrangements. Typically, hybridization generates individuals of low fitness due to genetic incompatibilities in the merging genomes, such as Dobzhansky-Muller genic interactions displaying negative epistasis (Orr and Turelli 2001; Mallet 2007). If structural differences exist between the chromosomes of the hybridizing genomes, they may impair proper meiosis and contribute to full or partial sterility. Overall, there exists a general relationship between genetic divergence, genome rearrangements, hybrid fitness, and reproductive isolation that is still poorly understood (Comeault and Matute 2018).

On the other hand, hybridization has the potential to facilitate adaptive evolution by bringing together novel allele combinations across loci that may produce novel phenotypes (Rieseberg *et al.* 1999; Dittrich-Reed and Fitzpatrick 2013). Particularly in plants, hybridization has led to the formation of new species, often through mechanisms such as allopolyploidization which avoids the sterility barrier concomitant with chromosomal rearrangements (Rieseberg 2001). Hybridization in fungi is increasingly recognized as having contributed to evolutionary novelty and host-range expansion (Schardl and Craven 2003; Marcet-Houben and Gabaldón 2015; Stukenbrock 2016; Samarasinghe *et al.* 2020a). However, there are many examples of fungal hybrids that appear to be restricted to the F1 diploid stage, such as the extremophile *Hortaea warneckii* (Gostinčar *et al.* 2018), *Epichlöe* endophytes (Saikkonen *et al.* 2016), *Aspergillus latus* (Steenwyk *et al.* 2020), and emerging pathogenic *Candida* spp. (Pryszcz *et al.* 2015; Schröder *et al.* 2016; Mixão and Gabaldón 2020). Because many fungi have the ability to reproduce asexually for extended numbers of generations, the F1 hybrid genotypes/species may generate transient, successful clonal lineages that avoid segregation load and chromosomal incompatibilities that may come with meiosis (Mallet 2007). Moreover, the

90 heterosis that occurs in diploid F1 hybrids might be particularly common, because multiple
91 mechanisms can contribute to it, such as complementation of recessive, mildly deleterious
92 alleles, overdominance, and epistasis (Shapira *et al.* 2014).
93 Despite the potential for overall heterosis in F1 hybrids, it is likely that such hybrid
94 genotypes contain a number of alleles or allelic interactions that reduce fitness, such as
95 incompatibilities driven by negative epistasis, underdominance, or gene copy number
96 imbalance. Given this situation, it is also likely that hybrids could undergo minor adaptive
97 changes in genotype through mitotic processes such as chromosome copy number variation
98 and loss of heterozygosity (LOH), which would allow genotypic change without wholesale
99 meiotic shuffling (Bennett *et al.* 2014; Samarasinghe *et al.* 2020a). LOH occurs through a
100 number of mechanisms, including gene conversion, nondisjunction, deletions, or crossing over
101 (St Charles *et al.* 2012; Symington *et al.* 2014). Overall, while it is clear that asexual F1 hybrids
102 are commonly observed in fungi, it is unclear how often and by what means they utilize their
103 allelic diversity for adaptation and relief of incompatibilities and whether these mechanisms can
104 allow asexual hybrids to persist for a long time despite Muller's Ratchet (Gabriel *et al.* 1993).
105 *Cryptococcus* is a model basidiomycete yeast that causes opportunistic infections
106 particularly in immunocompromised hosts. Most infections result from colonization by *C.*
107 *neoformans* (serotype A) with infection by *C. deneoformans* (serotype D) rare (Cogliati 2013).
108 These two species are diverged by at least ~24.5 mya (Xu *et al.* 2000b). In both clinical and
109 environmental settings, a large percentage (~8%) of *Cryptococcus* isolates are hybrid strains,
110 particularly those formed between *C. neoformans* and *C. deneoformans*, often referred to as AD
111 hybrids (Samarasinghe and Xu 2018). Studies with AD hybrids show variable virulence and
112 hybrid vigor relative to parental species, however, evidence for transgressive segregation in
113 pathogenicity relevant traits such as resistance to UV irradiation, growth at 37 C, and resistance
114 to antifungal drugs has been observed (Litvintseva *et al.* 2007; Lin *et al.* 2008; Vogan *et al.*
115 2016; Samarasinghe *et al.* 2020a).

116 Genomic plasticity is apparent in AD hybrids, but it is unclear which mechanisms are
117 most important for adaptation. Most AD hybrids are close to diploid and, although they produce
118 sexual spores in the lab, these appear to undergo an aberrant form of meiosis (Lengeler *et al.*
119 2001; Sun and Xu 2007; Hu *et al.* 2008; Vogan *et al.* 2013). The two species are 85-90%
120 divergent at the sequence level, and they are known to have karyotype differences (Kavanaugh
121 *et al.* 2006; Sun and Xu 2009). The dependence on sequence similarity for homology-based
122 recombination, such as the classical double strand break repair pathway (DSBR) is likely to be
123 inhibitory to mitotic and meiotic recombination at this level of sequence divergence (Datta *et al.*
124 1997; Opperman *et al.* 2004; Hum and Jinks-Robertson 2019). It was recently demonstrated
125 that deletion of the DNA mismatch repair gene *MSH2* did not increase the rate of homologous
126 recombination in meiotic progeny of an AD hybrid cross as observed in most other species but
127 did increase viability through increased aneuploidy, a result consistent with either sequence
128 dissimilarity or genetic incompatibility limiting recombination in *Cryptococcus* AD hybrids (Priest
129 *et al.* 2021). Reduced recombination may explain why genomic scale studies of naturally
130 occurring AD hybrids typically have primarily detected LOH of entire chromosomes (Hu *et al.*
131 2008; Li *et al.* 2012; Rhodes *et al.* 2017). A recent experimental evolution study of an AD hybrid
132 genotype showed that LOH of Chr. 1 could be rapidly stimulated if hybrids were grown in the
133 presence of the antifungal fluconazole, which has a major resistance allele encoded on Chr. 1 of
134 the *C. neoformans* parent (Stone *et al.* 2019; Dong *et al.* 2020). In this same study, LOH was
135 shown to occur at a rate of 6×10^{-5} per locus per mitotic division, and the distribution of LOH
136 was unequal across chromosomes. Little is known about the extent to which more spatially
137 restricted forms of LOH, such as gene conversion and mitotic crossing over have contributed to
138 LOH in natural AD hybrids. The precise mechanisms of LOH in most studies are masked due to
139 low numbers of markers utilized for genotyping, making it unclear whether the high level of
140 sequence diversity inhibits homologous recombination in *Cryptococcus* AD hybrids through anti-
141 recombination mechanisms.

142 In this study, we experimentally evolved AD hybrids to six distinct environments to test
143 which mechanisms of genomic change are involved in rapid adaptation. Using replicate
144 populations, both in liquid media and a model host (larvae of the waxworm moth *Galleria*
145 *mellonella*), we tested for evidence of parallel mutation, LOH, or copy number variation across
146 genes and chromosomes. Because of the divergence between parental alleles, we
147 hypothesized that unlike in *Candida albicans* (Ene *et al.* 2018) and *Saccharomyces cerevisiae*
148 (James *et al.* 2019) LOH would primarily be through nondisjunction of entire chromosomes
149 rather than via mechanisms that involve homologous recombination (e.g., gene conversion or
150 crossing over). Finally, we designed the experiment so that it would test whether particular
151 environments would favor one parental genotype than the other as previous investigations have
152 hinted at (Hu *et al.* 2008; Samarasinghe *et al.* 2020b). We found that whole chromosome LOH
153 and aneuploidy were common among the evolved clones in addition to de novo point mutations.
154 LOH events and aneuploidy demonstrated parallel evolution across independent cultures,
155 however, these parallel events were mostly environment agnostic. In concert with the
156 demonstration that the evolved strains have increased fitness, these data are consistent with
157 LOH occurring to reduce genetic incompatibilities between the two parental species (Vogan and
158 Xu 2014).
159
160 **Materials and Methods**
161
162 *Strains*
163 We initiated evolution starting with a single diploid hybrid strain generated by crossing *C.*
164 *neoformans* haploid strain YSB121 (KN99 *MAT***a** *aca1::NEO ura5 ACA1-URA5*) with *C.*
165 *deneoformans* strain SS-C890 (*MAT*α *NAT* ectopically inserted into a JEC21 genome and later
166 determined to be inserted in the sub-telomeric region of the left arm of Chr. 1). Over 100 diploid
167 products resistant to NAT and G418 (conferred by *NAT* and *NEO* genes present in the two

168 haploid parents) were identified that also produced extensive filamentation on V8 agar, a
169 phenotype characteristic of cells that are heterozygous that the mating type locus and have both
170 **a** and α *MAT* alleles. These were genotyped at 11 PCR markers across 6 chromosomes plus
171 the *MAT* locus (**Suppl. Table 1**) to identify highly heterozygous diploid offspring. The genotypes
172 of these markers were determined by size differences or presence/absence of a band (*STE20*
173 locus) using agarose gel electrophoresis. One of the diploids (SSD-719) heterozygous at all
174 markers was chosen as the ancestral genotype. A near isogenic strain (SSE-761) was
175 generated to serve as a reference competitor strain by random integration of a GFP-Nop1-*HYG*
176 cassette into SSD-719 (Park *et al.* 2016).
177
178 *Passaging in vitro*
179 Experimental passaging in five media types was conducted in parallel with a *Saccharomyces*
180 *cerevisiae* evolution experiment (James *et al.* 2019). Briefly, 6 replicate populations of 500 μl
181 were inoculated with the hybrid ancestor strain, grown at 30 °C with shaking, and transferred
182 daily with 1/50 dilution into new media. The media types were yeast peptone dextrose (YPD),
183 beer wort, wine must, YPD + high salt (1 M NaCl), and minimal medium plus canavanine
184 (James *et al.* 2019). Every fifth passage, 25 μl of each population was subsampled for archiving
185 in 25% glycerol at -80 °C. At the end of 100 days, one clone was isolated from each population
186 by streak plating, and the remaining population archived.
187
188 *Passaging in vivo*
189 We utilized last instar larvae of *Galleria mellonella* for the infection model with inoculation and
190 incubation following (Phadke *et al.* 2018). Six replicate populations of 5 larvae were founded,
191 with each larva injected with 10^7 cells. Larvae were incubated 5 days with ambient temperature
192 and lighting. The larvae were then crushed in 50 ml sterile water and 50 μl were plated onto

193 three 15 cm plates of YPD containing 200 mg/L G418 and 200 mg/L ampicillin. After 72 hr of
194 incubation, the plates containing on the order of 10^3-10^4 small colonies were scraped and
195 pooled into 50 ml of sterile water, the cell density was adjusted to the appropriate level (10^6/μl)
196 for inoculation, and the next population of 5 larvae was inoculated. After 10 passages in this
197 manner, a single clone from each population was isolated for analysis.
198
199 *Fitness estimation*
200 We estimated fitness of our evolved strains using both growth curves and competition with a
201 reference strain. Growth curves were estimated using a Bioscreen C (Growth Curves USA)
202 following James *et al.* (2019). Competition-based fitness was measured by comparing
203 proportions of unlabeled cells (evolved) with a near isogenic competitor strain (SSE-761)
204 engineered to express GFP. Mixtures of the competitor strain and evolved strain were analyzed
205 for green fluorescent events to non-fluorescent events both before and after growth on a iQue
206 Screener PLUS (Intellicyt) according to James *et al.* (2019). Each pairwise competition was run
207 using 8 replicate populations.
208
209 Fitness was also estimated in the *Galleria*-passaged clones as well as two clones isolated from
210 beer wort. *In vivo* fitness of the evolved strains was estimated by co-injection of evolved with
211 competitor strain SSE-761 as a combination of 2 x 10^6 cells in 10 μl into each of 5 larvae. After
212 incubation for 48 hrs at ambient temperature, larvae were crushed in sterile water, filtered
213 through a 40 μm filter, and plated on two media types: YPD media containing G418 (200 mg/L),
214 ampicillin (200 mg/L), and chloramphenicol (25 mg/L), and YPD media containing the same
215 antibiotics plus hygromycin (200 mg/L) and incubated at 30 °C until colony development. The
216 latter media type only permits growth of the competitor strain while the former allows growth of
217 both evolved and competitor. We also plated the mixture of evolved and competitor strains on

218 the two media types to measure the ratio of the genotypes pre-injection. All experiments were
219 repeated three independent times. Colony sizes varied considerably, and in order to count the
220 colonies in a rapid, objective manner, we used the program OpenCFU (Geissmann 2013) using
221 a threshold of 5 and a minimum radius of 20. By comparison of the ratios of the two genotypes
222 pre- and post-infection, fitness can be measured. Fitness (*F*) values were calculated using
223 colony counts on G418-only media pre- (G_{pre}) and post-infection (G_{post}) and colony counts on
224 G418+hygromyin media pre- (H_{pre}) and post-infection (H_{post}) using the following formula:

225 $$F = \frac{G_{post}/H_{post}}{G_{pre}/H_{pre}}$$

226 We presented the mean *F* for each clone as a relative fitness measure by dividing by the mean
227 *F* estimate the competition between the ancestral genotype vs. congenic competitor strain.
228
229 *Genome resequencing*
230 DNA was extracted from clones grown overnight in 2 ml of YPD following (Xu *et al.* 2000a). One
231 clone from each population was sequenced, for a total of 35 clones (library of CB-100-4 failed to
232 pass QC). The ancestral haploid and diploid parents were also sequenced. Because the clones
233 evolved via passaging in *Galleria* were initiated after the *in vitro* evolution experiment using a
234 separate subclone of the ancestor, we also sequenced the two ancestral diploid genotypes
235 separately. Poor DNA extraction of the SSD-719 *in vivo* culture required a second DNA
236 extraction, which resulted in additional opportunities for genomic change. Libraries for genome
237 sequencing were constructed with dual indexing using 0.5-2.5 ng per reaction using a Nextera
238 XT kit (Illumina). The libraries were multiplexed and sequenced on an Illumina HiSeq 2500 v4 or
239 NextSeq sequencer using paired end 125 bp output. After analyses the expected coverage for
240 each strain ranged from 41-147X.
241
242 *Data analyses*

243 The full pipeline, including scripts and data sets used for analysis of the genomic data can be
244 found at https://github.com/Michigan-Mycology/Cryptococcus-LOH-paper, with larger variant call
245 format (vcf) files stored using figshare. Details of the variant calling pipeline using GATK 4.0.0
246 (McKenna *et al.* 2010) are similar to James *et al.* (2019). Briefly, data were trimmed for quality
247 using Trimmomatic 0.36 (Bolger *et al.* 2014). The genomes of the two parental haploid strains
248 backgrounds (JEC21 (Loftus *et al.* 2005), H99 (Janbon *et al.* 2014)) were downloaded and
249 aligned using Harvest (Treangen *et al.* 2014). The variants from these alignments were used as
250 a set of known variants in the base recalibration step of GATK. SNP identification for LOH and
251 de novo mutation analyses was done using HaplotypeCaller using the H99 genome as the
252 reference. After variant filtration for quality in GATK, SNPs were converted into a vcf file and
253 further filtered. Genotypes were set to unknown when their depth was < 18X or > 350X, the
254 genotype quality (GQ) was < 99, or the sites were not present as differences between the
255 haploid ancestors observed as heterozygosity in the diploid ancestor. SnpEff 4.3K (Cingolani *et*
256 *al.* 2012) was used to assign functional information to SNPs. We scanned for new mutations
257 occurring during passaging using the criteria that they were absent in both haploid parents and
258 ancestral diploid strain and appeared with sequencing depth > 18X and GQ >= 99. Estimating
259 the number and length of each LOH event was done using the custom perl script
260 calculate_LOH_lengths_crypto_100_new.pl. After identifying LOH patterns, we later verified
261 each event by examining the read pileup and vcf file and excluded LOH events which were not
262 supported by 100% of reads as homozygous. We removed single SNP LOH events, because
263 they showed strong association of reads linked to only a single allele in flanking heterozygous
264 SNPs, indicating they are likely false positives. Indels were ignored for considering LOH, which
265 underestimates the overall amount of LOH and allelic diversity, but should not cause systematic
266 biases in hypothesis testing.
267

268 We identified aneuploidy by mapping reads to a combined AD hybrid reference as in Priest *et al.*
269 (2021). In this hybrid reference sequence, the *C. deneoformans* chromosomes have been
270 reordered and reverse-complemented where necessary to better match the chromosome order
271 of *C. neoformans*. The trimmed reads of each strain were mapped using bwa v. 0.7.15 (Li and
272 Durbin 2009), reads of low mapping quality (-q 3) removed using samtools v. 1.5 (Li *et al.* 2009),
273 and coverage estimated along chromosomes in 5 kb intervals with bedtools v. 2.29.2 (Quinlan
274 and Hall 2010). The data were then plotted using ggplot2 (Wickham 2009) after removal of
275 windows with depth of coverage > 5X the genome-wide average. Local scale copy number
276 variation (CNV), specifically looking for deletions, was evaluated using the software smoove
277 (https://github.com/brentp/smoove).
278
279 All statistical analyses and plots were conducted in R 3.6.2 (R_Core_Team 2019) unless
280 otherwise specified. Most statistical tests utilized the base package; we also utilized the
281 functions ggplot2 and gridextra for graphical output (Auguié 2017).
282
283 *Data availability*
284 Strains and plasmids are available upon request. The full pipeline, including scripts and data
285 sets used for analysis of the genomic data, additional data files, and code for reconstructing
286 figures can be found on Github (https://github.com/Michigan-Mycology/Cryptococcus-LOH-
287 paper). Raw sequence data has been deposited into NCBI's SRA archive under BioProject:
288 PRJNA700784, with the accession numbers SRX10055646-SRX10055684.
289
290 **Results**
291
292 *Fitness estimates suggest adaptation during passaging*
293

294 We evolved a single AD hybrid genotype (SSD-719) in 5 *in vitro* environments by serial transfer
295 for 100 days and also evolved the genotype through 10 serial passages in waxworm larvae. The
296 experiment was run in parallel with an investigation of microevolution in *Saccharomyces*
297 *cerevisiae*, and while the media types are more typical for brewing yeast, they served to
298 represent broadly diverse environments that would require adaptation by the laboratory-created
299 *Cryptococcus* hybrids. Each environment was represented by 6 replicate populations, and from
300 each of these evolved populations we isolated individual clones, determined whether they had
301 evolved a higher fitness relative to the ancestral genotype, and sequenced their genomes. The
302 6 clones isolated after evolution in each *in vitro* environment generally showed increased fitness
303 relative to the ancestral genotype (**Figure 1**). Maximal population density (EOG) and
304 competitive fitness mostly increased for all strains and environments, whereas doubling time
305 was lower for clones evolved in high salt or canavanine environments.
306
307 The virulence and relative fitness of the *G. mellonella* passaged strains was estimated for the 6
308 clones that had been serially passaged 10 times in the same host compared with the ancestral
309 diploid genotype and isolates that had been evolved in beer wort. The larval passaged strains
310 showed enhanced survivorship (one-way ANOVA, [$F(8,18)=3.59$, $P=0.0115$]) compared to the
311 beer wort evolved and ancestral strain as measured by genotype recovery after co-injection with
312 a marked strain (**Figure 2**).
313
314 *Parallel LOH was observed mostly as whole chromosome loss in a non-environment specific*
315 *manner*
316
317 LOH was readily apparent at the chromosome scale (**Figure 3**), suggesting that most strains
318 had undergone chromosome-scale LOH events as well as multiple smaller events. We
319 estimated that strains had undergone an average of 2.9 LOH events after 100 days,

320 encompassing an average of 2.26 Mbp. There was a significant difference between the average
321 number of LOH events across environments (Kruskal-Wallis test, $X^2(5) = 18.26$, $p = 0.026$), but
322 these differences were driven mostly by low LOH numbers in larval passaged strains (beer wort:
323 2.8, canavanine: 4.2, high salt: 1.8, wine must: 2.7, YPD: 4.7, larvae: 0.8). Most of the LOH
324 events were the result of whole chromosome events, with the second most common being long
325 distance LOH consistent with break-induced replication (BIR) observed as crossing over not
326 associated with gene conversion, followed by gene conversion, and then deletions (**Figure 4**).
327 Crossover and deletion events averaged 173 kb in total length, and gene conversions averaged
328 7.4 kb.
329
330 We looked for evidence that specific LOH events showed parallel evolution across
331 independently evolved clones. We specifically noted parallel changes as regions of the genome
332 undergoing LOH in 3 or more clones. Among the LOH events, 11 were found in more than 3
333 clones, including whole chromosome or long distance LOH on Chr. 2, 4, 9 and 12 (**Figure 3**).
334 The other regions were limited to only 3 clones. There was no evidence for any of the LOH
335 events being more predominant in particular environments.
336
337 We asked whether whole-chromosome LOH events favored one parental type over another,
338 which was obvious for Chr. 2 in which LOH exclusively led to retention of the *C. deneoformans*
339 homolog. For the 4 chromosomes (2, 4, 9 and 12) with 4 or more independent LOH events we
340 tested whether the allelic distribution of homozygotes was non-random or skewed towards one
341 parent. Although events at most chromosomes favored one parental genotype over another,
342 only the Chr. 2 pattern was significant (P=8.2e-06; Fisher's exact test).
343
344 We then tested whether one of the parental genotypes was globally favored over the other
345 across isolates by asking whether the ratio between SNP loci that are homozygous for the

346 *neoformans* and *deneoformans* alleles, respectively, deviated significantly from a random 1:1
347 null hypothesis. Overall, we found that the mean frequency of *neoformans* alleles in LOH
348 regions across all evolved clones was 0.234 (CI: 0.115-0.353), which was significantly different
349 from the null hypothesis (t(34) = -4.61, p = 7.0e-5). However, if Chr. 2 was excluded, the mean
350 frequency of *neoformans* alleles in LOH regions was 0.639 (CI: 0.488-0.791), which was not
351 significantly different from the null expectation ($t(34) = 1.88$, $p = 0.070$). These data suggest
352 there is no signal of a favored parental allele arising from the LOH process with the exception of
353 LOH favoring retention of the *C. deneoformans* Chr. 2 homolog.
354
355 Using the rate of LOH events uncovered and their sizes, we estimated a rate of 0.005
356 events/generation, 4.0 kb/generation, and 2×10^{-4} per bp per generation. Dong et al. (2019)
357 estimated a rate of LOH of 6×10^{-5} per locus per mitotic division with 33 loci in *Cryptococcus* AD
358 hybrids, leading to an estimation of 0.002 LOH events per generation.
359
360 *Prevalence of aneuploidy across passaged isolates*
361
362 Aneuploidy leading to chromosomal copy number variation is a rapid means with which
363 pathogenic fungi generate adaptive genetic variation (Bennett *et al.* 2014; Beekman and Ene
364 2020). We tested for the presence of both whole chromosomal and partial chromosomal
365 aneuploidy by using the density of reads mapped to a hybrid version of the genome, which we
366 found to give a clearer picture of depth of coverage than solely using one species reference
367 genome. The mapping data also provided strong confirmation of our LOH results. Most of the
368 strains had mapping patterns that fell into distinct chromosome counts of 0-3, with a few cases
369 in which average mapping density appeared to be intermediate, a result consistent with ongoing
370 chromosome loss in strains used for genome sequencing (**Figure 5**). We found that the evolved
371 strains often showed aneuploidy on multiple chromosomes (**Figure 6**; **Suppl. Figures 1-6**). In

372 all cases, aneuploidies were trisomies and no evidence of monosomies was found. Particular
373 chromosomes (Chr. 2, 4, 9, 10, and 11) were likely to display aneuploidy and were strikingly
374 overlapping with the same chromosomes that had also undergone whole chromosome LOH
375 (**Figure 3**). Among the evolved lines, there was a 2:1 bias towards trisomies that involved extra
376 copies of the *C. deneoformans* homeologue. Some aneuploidies were also present in the
377 ancestral diploid but not haploid genotypes (**Suppl. Figure 6**). For example, Chr. 9 was trisomic
378 in all larval passaged clones, but was also observed in the *in vivo* diploid ancestor, although
379 most passaged strains maintained heterozygosity on Chr. 9 unlike the ancestor. Chr. 3 of *C.*
380 *deneoformans* was duplicated in the *in vitro* ancestor, but most of the evolved strains did not
381 have this aneuploidy (**Figure 6**). Clone CW-100-4 evolved in wine must revealed a complex
382 pattern of chromosome ploidy consistent with either multiple subpopulations within the strain
383 with different aneuploidies or possibly a primarily tetraploid strain (**Suppl. Figure 3**). Overall,
384 there were 25 aneuploidies that uniquely appeared after passaging, for 0.7 events per clone.
385
386 Chr. 2 shows a complex history after the creation of the hybrid ancestor by mating in the lab.
387 Both *in vitro* and *in vivo* ancestors show a deletion on the right arm of *C. neoformans* Chr. 2,
388 spanning ~260 kb. This was accompanied by a duplication of the entire *C. deneoformans*
389 homeologue in the *in vitro* ancestor and a partial duplication of the *C. deneoformans*
390 homeologue in the *in vivo* ancestor. Most of the *in vitr*o evolved strains ultimately lost the
391 *neoformans* Chr. 2 homeologue, however, it was retained in clones CW-100-6, CY-100-3, CY-
392 100-6, and in part in CY-100-1 (**Suppl. Figures 3-4**). The loss of the *C. neoformans* Chr. 2
393 homeologue may have been advantageous to the strains; strains CY-100-3 and CY-100-6 that
394 retained the *C. neoformans* homeologue had the two lowest fitness values for YPD evolved
395 strains in two fitness measures (doubling time and relative fitness versus competitor).
396

397 Most of the trisomies did not show an environment specific pattern, however, trisomy derived via
398 duplication of the Chr. 11 *C. deneoformans* homeologue was present in all beer wort evolved
399 strains and one strain evolved in canavanine. This trisomy was significantly associated with
400 beer wort (Fisher's exact test, P=8.6e-05), suggesting this association may have been driven by
401 an environment-specific fitness advantage of this extra chromosome.
402
403 Chromosome plots and a structural variant detection method (smoove) were also employed to
404 detect partial aneuploidy occurring via partial chromosomal deletion. Seven LOH events were
405 consistent with deletions (2 identified by smoove and 5 visually from relationship of coverage
406 with LOH events). Overall, these data suggest that most strains are not diploid but instead
407 aneuploid with duplication of the *C. neoformans* homeologue more frequently involved in
408 trisomies of particular chromosomes.
409
410 *Absence of parallel evolution by point mutations*
411
412 We found 117 high quality *de novo* mutations at 93 SNP loci specifically occurring in the
413 evolved clones that were absent from both haploid and diploid ancestors. The mean number of
414 mutations per strain was 3.3 (range 0-10), and mutations were found on every chromosome and
415 in every environment type. The majority of the mutations were inside exons (81.7%), with the
416 remaining intronic (10.8%), or intergenic (8.5%). Most of the mutations in exons had
417 consequences on the protein sequence, with 64.5% missense, 6.6% nonsense, and 28.9%
418 synonymous (**Suppl. Table 2**). Of 117 mutations only 4 of them were found as homozygous
419 genotypes. Because a number of chromosomes have undergone whole chromosome or long
420 distance LOH, the fact that most mutations are heterozygous implies that whole chromosome
421 LOH likely occurred early on during the evolution of the populations, followed by mutations.
422

423 Of the 93 *de novo* single nucleotide mutation loci, only 3 were found in 3 or more strains. Three
424 loci showed 3, 7, and 8 strains bearing the mutation. These were all mutations of low impact
425 and may represent variation in the initial founding population that became fixed during evolution.
426 Mutations with protein-altering effects were found in diverse genes, including transcription
427 factors, plasma-membrane proton-efflux P-type ATPase, and many others. A test for enrichment
428 of Gene Ontology terms among the protein-altering mutations using clusterProfiler (Yu *et al.*
429 2012) identified lipid metabolic process as the most enriched term, although this enrichment is
430 not statistically significant after correction for multiple testing (FDR corrected P = 0.103).
431
432 *Relationship of LOH break points to sequence divergence and mutation*
433
434 The ability to undergo crossing over is known to be influenced by anti-recombination
435 mechanisms that prohibit recombination due to sequence divergence. Such a mechanism would
436 favor mitotic recombination breakpoints in regions of lower divergence. We found no
437 relationship between heterozygosity of particular chromosomes and the number of crossover
438 events observed (r(12) = 0.083, p = 0.78; **Suppl. Table 3**). By plotting the locations of mitotic
439 recombination breakpoints and mutations relative to chromosomal divergence (**Figure 7**),
440 however, we identified a clear pattern that many of the breakpoints are sub-telomeric, and sub-
441 telomeric regions often have lower divergence between the two parents. We tested whether the
442 heterozygosity near crossing over breakpoints was depressed relative to random breakpoints
443 produced in simulated data sets. In total there were 47 independent breakpoints observed (only
444 the left breakpoint was used for gene conversion events). For windows of size 1000 bp centered
445 around the breakpoints, the mean post-filtering heterozygosity of the windows was 0.026. From
446 1000 simulated data sets, the mean simulated divergence near random breakpoints was much
447 higher (0.045), with a range of 0.037-0.051, providing a highly significant (P<0.001) difference
448 between heterozygosity near observed breakpoints to randomly chosen ones. Varying the

449 window size from 30-10^5 bp revealed that heterozygosity near LOH breakpoints was lower than
450 the random expectation for every case (P<0.001). This result suggests that recombination in
451 *Cryptococcus* AD hybrids is favored in broad regions of lower divergence between recombining
452 genomes.
453
454 We investigated the breakpoints further to understand if there were sequence characteristics
455 that promoted recombination and identified hotspots at two regions of the *Cryptococcus* genome
456 where ancestral introgression likely occurred between the two parental lineages (Kavanaugh *et*
457 *al.* 2006). The smaller of the introgression events encompasses ~12 kb of the left arm of *C.*
458 *neoformans* Chr. 10 which is found on the right arm of Chr. 13 in *C. deneoformans*. This small
459 region of ~5% sequence divergence harbored 3 of the 47 independent breakpoints. The
460 second, larger introgression event is a 40 kb region found in a sub-telomeric region of the left
461 arm of *C. neoformans* Chr. 5 which was apparently the parent of a non-reciprocal introgression
462 and translocation into *C. deneoformans*. Strikingly, 4/6 non-whole chromosome LOH events
463 occurring on *C. neoformans* Chr. 5 have a crossover event in this "identity island". Two of these
464 events are gene conversions with one end near the boundary of the island where one partial
465 copy of the non-LTR retrotransposon Cnl1 is present.
466
467 In *Candida albicans*, a positive relationship has been observed between mitotic recombination
468 and *de novo* mutation (Ene *et al.* 2018), indicative of recombination-induced mutagenesis as
469 observed in meiosis in yeast and other organisms (Arbel-Eden and Simchen 2019). We tested
470 for such a relationship by comparing the relative distance of observed mutations to crossover
471 locations to a simulated set of random mutations in the genome (1,000 simulations). This result
472 supports the overview in **Figure 7** that suggests there is no clear relationship between *de novo*
473 mutation and crossover events in *Cryptococcus* AD hybrids (P = 0.508).
474

475 **Discussion**

476

477 Mutations are the primary way in which clonal organisms evolve. However, there are additional
478 avenues for genetic change in clonal organisms referred to as genome plasticity, which are
479 particularly available to polyploid hybrid genomes (Albertin and Marullo 2012; Blanc-Mathieu *et*
480 *al.* 2017; Samarasinghe *et al.* 2020a). In this study we investigated the sources of genetic
481 variation in evolving hybrid strains of *Cryptococcus* continuously passaged in differing
482 environments. Passaging led to adaptation as observed by increased fitness of the clones
483 isolated at the end of the experiment relative to the ancestral genotype. Genome resequencing
484 allowed an unprecedented look at lab-evolved *Cryptococcus* hybrids and revealed multiple
485 mechanisms of genomic change. Genomic plasticity was observed as chromosome copy
486 number amplification and LOH generated via nondisjunction, gene conversion, and crossing
487 over. However, the location of these genome scale events is highly biased across the genome,
488 occurring in particular chromosomal locations presumably deeply influenced by the history of
489 the divergence of the two sibling species.

490

491 This experiment was conducted at the same time as a similar passaging experiment using
492 *Saccharomyces cerevisiae* (James *et al.* 2019), and therefore the media conditions were
493 atypical for *Cryptococcus*. Therefore, it is unsurprising that the *Cryptococcus* hybrid genotype
494 improved significantly in fitness over the period of evolution, particularly as measured by density
495 at carrying capacity (EOG) and in head-to-head competition with the ancestor (**Figure 1, B-C**).
496 *Cryptococcus* AD hybrids had a lower average LOH rate (2.9 event/100 days) relative to *S.*
497 *cerevisiae* (5.2 events/100 days), despite the same dilution rate on transfer and hence
498 equivalent number of generations. Moreover, the mechanism of LOH in *Cryptococcus* AD
499 hybrids was very different than that of *S. cerevisiae* heterozygous diploids. Specifically, LOH in
500 *Cryptococcus* is dominated by nondisjunction of chromosomes, while LOH in *S. cerevisiae* had

501 gene conversion as the majority mechanism and no evidence of whole chromosome LOH. Both
502 fungi had LOH consistent with crossing over or BIR (**Figure 4**; Class 4), but *S. cerevisiae* had
503 considerably more crossing over associated with gene conversion, consistent with the classical
504 double strand break repair model (Symington *et al.* 2014). A major difference that may explain
505 this pattern is that the initial heterozygosity of the ancestral diploid genotypes of *Saccharomyces*
506 was 0.005-0.009 or one heterozygous position out of every 100. In our highly filtered
507 *Cryptococcus* data set, we considered 5.6e05 heterozygous positions in the AD hybrids (0.03
508 heterozygosity), however, it is known that *C. neoformans* and *C. deneoformans* are 85-90%
509 divergent at the sequence level (Kavanaugh *et al.* 2006; Sun and Xu 2009) making differences
510 on the order of 10 bases for every 100.
511
512 LOH and aneuploidy was highly heterogeneous across the *Cryptococcus* genome. Whole
513 chromosome LOH was primarily observed on chromosomes 2, 4, and 9, and trisomy was
514 common for these chromosomes plus 10 and 11. Comparison of *C. neoformans* to *C.*
515 *deneoformans* has identified 32 chromosomal rearrangements (Sun and Xu 2009). Most of
516 these are smaller inversions or complex rearrangements, while a few of them represent large
517 chromosomal changes, such as multiple translocations and inversions between chromosomes 3
518 and 11. The rearrangement between Chr. 3 and 11 had a severe and suppressive impact on
519 long distance LOH both as whole chromosome loss or as crossover events, however these
520 chromosomes may still play a role in adaptation through chromosomal copy number changes,
521 and one amplification (Chr. 11 of *C. deneoformans*) was positively associated with growth in
522 beer wort. Other larger chromosomal rearrangements likely had additional suppressive effects
523 on the ability of the homologous chromosomes to undergo mitotic recombination. For example,
524 no crossover events were observed on the right arm of chromosome 9, which is expected due
525 to the large inversion between *C. neoformans* and *C. deneoformans* in this region (Sun and Xu
526 2009).

527

528 If sequence dissimilarity and chromosome rearrangements hinder mitotic recombination what
529 might stimulate it? Crossover locations were highly biased towards sub-telomeric regions, and
530 these are regions where there are fewer heterozygous mapped positions. It is worth pointing
531 out, however, that there are multiple explanations for lower heterozygosity at the telomeric
532 regions. One could be hemizygosity at these regions, or alternatively the enrichment of
533 repetitive DNA elements such as transposons in these regions (Loftus *et al.* 2005), which
534 remain unmapped with short read technology. It is clear that there is an association between
535 transposable elements and chromosomal rearrangement and introgression (Kavanaugh *et al.*
536 2006; Sun and Xu 2009). We found that regions of lower divergence caused by transposable
537 element-associated introgression were hotspots of mitotic recombination. These results allude
538 to a scenario in which the transposable elements both speed up and slow down the speciation
539 process by both increasing genome rearrangements but also increasing genetic similarity
540 through introgression, which should increase the ability to recombine.

541

542 While this experiment played out over a mere ~500 generations, naturally occurring hybrids
543 reveal evolutionary processes occurring over much longer time periods. *Cryptococcus* AD
544 hybrids have arisen multiple times independently and may have undergone clonal evolution for
545 up to 2 million years (Xu *et al.* 2002; Litvintseva *et al.* 2007). The results of our microevolution
546 study show many similarities to genomic analysis of the natural hybrids. For example, these
547 studies have observed both whole chromosome LOH and aneuploidy (Hu *et al.* 2008; Sun and
548 Xu 2009; Li *et al.* 2012; Rhodes *et al.* 2017). The specific chromosomes involved, however, are
549 different. While there are shared whole chromosome LOH events between our study and others
550 as in loss of the C*. deneoformans* Chr. 9 homolog or loss of the *MAT* encoding Chr. 4 (Sun and
551 Xu 2009; Li *et al.* 2012; Rhodes *et al.* 2017), the general pattern across strains and studies is
552 mostly stochastic, which contrasts with the highly deterministic pattern seen for Chr. 2 in our

553 experimental population. A possible explanation is that the hybridization events are
554 independent, and all of a different background than the lab generated one used in this study.
555 Many hybrids have the VNB lineage as the *C. neoformans* parent, but in our study the *C.*
556 *neoformans* parent was VNI (Litvintseva *et al.* 2007; Li *et al.* 2012). Another possibility is that
557 the LOH events observed are both stochastic yet contingent on existing genotype. Specifically,
558 our ancestral genotype lost the right 260 kb of the *C. neoformans* Chr. 2 before passaging. This
559 event may have set up a scenario where further loss of the entire *C. neoformans* Chr. 2 was
560 favored, perhaps due to genetic incompatibilities between genes on this chromosome.
561
562 Genomic plasticity via LOH and aneuploidy are predicted to be adaptive, though this must be
563 contrasted with a more neutral model. In the case of drug resistance in AD hybrids aneuploidy
564 and increased copy number is clearly selected for through amplification of resistance genes (Li
565 *et al.* 2012; Rhodes *et al.* 2017; Dong *et al.* 2020). Aneuploidy may merely be a byproduct of the
566 fact that chromosomal loss or duplication is the fastest means of achieving copy number change
567 or homozygosity of a single gene. That selection was responsible for the rapid increase in
568 homozygosity of Chr. 2 to the *C. deneoformans* homolog is supported by the fitness values of
569 strains without homozygosity of the Chr. 2 *C. deneoformans* homolog. These data are also
570 consistent with the strong bias towards the *C. deneoformans* parent of Chr. 2 in a large sample
571 of sexually recombined progeny from an AD hybrid of similar genetic background (Sun and Xu
572 2007), hinting that there may exist incompatibilities between genes from the two species on this
573 chromosome as predicted by the Dobzhansky-Muller model. Such intra- and inter-chromosomal
574 incompatibilities have been detected in a previous study of AD hybrids, suggesting that this a
575 plausible explanation (Vogan and Xu 2014). Alternatively, rather than epistatic interactions,
576 dosage or RNA/protein titer could differ between products encoded by the two parental
577 homologs, and this could provide opportunities for selection to act. For example, if there are
578 genes not present on Chr. 2 of *C. neoformans* that exist in *C. deneoformans* or if the expression

579 level of the *C. deneoformans* genes on Chr. 2 is more optimal, this could lead to selection
580 favoring loss of the *C. neoformans* homolog. As Chr. 2 is the chromosome containing the
581 ribosomal RNA (rRNA) array, we might hypothesize that either copy number or expression of
582 these genes could be involved in rapid whole chromosome LOH.
583
584 Overall, the contrasting results in LOH rate and mechanism between *Cryptococcus* hybrids and
585 *Saccharomyces* diploids (James *et al.* 2019; Sui *et al.* 2020) suggest that LOH in *Cryptococcus*
586 hybrids is comprised largely of whole chromosome events in part because of the inability for
587 *Cryptococcus* AD hybrids to undergo recombination. This evidence comes from the association
588 between crossover breakpoints and regions of lower heterozygosity, such as identity islands
589 shaped by introgression, an observation consistent with literature showing mitotic and meiotic
590 recombination is reduced in species with higher heterozygosity (Opperman *et al.* 2004;
591 Seplyarskiy *et al.* 2014; Hum and Jinks-Robertson 2019; Tattini *et al.* 2019). Hybrid linkage
592 maps also support suppression of recombination in *Cryptococcus* AD hybrids (Sun and Xu
593 2007; Vogan *et al.* 2013). In contrast, intraspecific linkage maps constructed using *C.*
594 *deneoformans* showed results comparable to *S. cerevisiae* (~5 kb/cM) (Cherry *et al.* 1997;
595 Forche *et al.* 2000; Sun *et al.* 2014; Roth *et al.* 2018), revealing that homologous recombination
596 is not generally inhibited in the genus. Rates of mitotic recombination within *Cryptococcus*
597 intraspecific crosses have not been measured. In our study design, we also evolved *C.*
598 *deneoformans* diploids that were completely homozygous. These homozygous diploid
599 populations showed a similar rapid increase in fitness as evolved *Cryptococcus* hybrid clones,
600 and future genome sequencing could resolve whether most *de novo* mutations remain
601 heterozygous as observed in hybrid clones or may have undergone LOH at a higher rate.
602
603
604

Acknowledgements

This work was made possible by grants from the National Institutes of Health, National Institute of Allergy and Infectious Diseases (5R21AI105167-02, R37 AI39115-24, and R01 AI50113-16). J.H. is co-director and he and T.Y.J. are fellows of CIFAR program Fungal Kingdom: Threats & Opportunities. We thank Emmi Mueller and Ellen James for technical lab support. We thank Marco Coelho for providing the hybrid reference genome and the schematics of the *Cryptococcus* chromosomes.

Literature Cited

Albertin W., and P. Marullo, 2012 Polyploidy in fungi: evolution after whole-genome duplication. Proceedings of the Royal Society B: Biological Sciences 279: 2497–2509. https://doi.org/10.1098/rspb.2012.0434

Arbel-Eden A., and G. Simchen, 2019 Elevated mutagenicity in meiosis and its mechanism. BioEssays 41: 1800235. https://doi.org/10.1002/bies.201800235

Auguié B., 2017 gridExtra: Miscellaneous Functions for “Grid” Graphics. R package version 2.3. https://CRAN.R-project.org/package=gridExtra.

Beekman C. N., and I. V. Ene, 2020 Short-term evolution strategies for host adaptation and drug escape in human fungal pathogens. PLOS Pathogens 16: e1008519. https://doi.org/10.1371/journal.ppat.1008519

Bennett R. J., A. Forche, and J. Berman, 2014 Rapid mechanisms for generating genome diversity: whole ploidy shifts, aneuploidy, and loss of heterozygosity. Cold Spring Harb Perspect Med 4: a019604. https://doi.org/10.1101/cshperspect.a019604

Blanc-Mathieu R., L. Perfus-Barbeoch, J.-M. Aury, M. Da Rocha, J. Gouzy, *et al.*, 2017 Hybridization and polyploidy enable genomic plasticity without sex in the most devastating plant-parasitic nematodes. PLoS Genet 13: e1006777. https://doi.org/10.1371/journal.pgen.1006777

631 Bolger A. M., M. Lohse, and B. Usadel, 2014 Trimmomatic: a flexible trimmer for Illumina
632 sequence data. Bioinformatics 30: 2114–2120.
633 https://doi.org/10.1093/bioinformatics/btu170
634 Cherry J. M., C. Ball, S. Weng, G. Juvik, R. Schmidt, *et al.*, 1997 Genetic and physical maps of
635 Saccharomyces cerevisiae. Nature 387: 67–73.
636 Cingolani P., A. Platts, L. L. Wang, M. Coon, T. Nguyen, *et al.*, 2012 A program for annotating
637 and predicting the effects of single nucleotide polymorphisms, SnpEff: SNPs in the
638 genome of Drosophila melanogaster strain w(1118); iso-2; iso-3. Fly 6: 80–92.
639 https://doi.org/10.4161/fly.19695
640 Cogliati M., 2013 Global molecular epidemiology of Cryptococcus neoformans and
641 Cryptococcus gattii : An atlas of the molecular types. Scientifica 2013: 1–23.
642 https://doi.org/10.1155/2013/675213
643 Comeault A. A., and D. R. Matute, 2018 Genetic divergence and the number of hybridizing
644 species affect the path to homoploid hybrid speciation. PNAS 115: 9761–9766.
645 https://doi.org/10.1073/pnas.1809685115
646 Datta A., M. Hendrix, M. Lipsitch, and S. Jinks-Robertson, 1997 Dual roles for DNA sequence
647 identity and the mismatch repair system in the regulation of mitotic crossing-over
648 in yeast. Proc Natl Acad Sci U S A 94: 9757–9762.
649 Dittrich-Reed D. R., and B. M. Fitzpatrick, 2013 Transgressive Hybrids as Hopeful Monsters.
650 Evol Biol 40: 310–315. https://doi.org/10.1007/s11692-012-9209-0
651 Dong K., M. You, and J. Xu, 2020 Genetic changes in experimental populations of a hybrid in
652 the Cryptococcus neoformans species complex. Pathogens 9: 3.
653 https://doi.org/10.3390/pathogens9010003
654 Ene L. V., R. A. Farrer, M. P. Hirakawa, K. Agwamba, C. A. Cuomo, *et al.*, 2018 Global analysis
655 of mutations driving microevolution of a heterozygous diploid fungal pathogen. Proc.
656 Natl. Acad. Sci. U. S. A. 115: E8688–E8697. https://doi.org/10.1073/pnas.1806002115

657 Forche A., J. Xu, R. Vilgalys, and T. G. Mitchell, 2000 Development and characterization of a
658 genetic linkage map of Cryptococcus neoformans var. neoformans using amplified
659 fragment length polymorphisms and other markers. Fungal Genet Biol 31: 189–203.
660 https://doi.org/10.1006/fgbi.2000.1240
661 Gabriel W., M. Lynch, and R. Bürger, 1993 Muller's ratchet and mutational meltdowns. Evolution
662 47: 1744–1757. https://doi.org/10.1111/j.1558-5646.1993.tb01266.x
663 Geissmann Q., 2013 OpenCFU, a new free and open-source software to count cell colonies and
664 other circular objects. PLOS ONE 8: e54072.
665 https://doi.org/10.1371/journal.pone.0054072
666 Gostinčar C., J. E. Stajich, J. Zupančič, P. Zalar, and N. Gunde-Cimerman, 2018 Genomic
667 evidence for intraspecific hybridization in a clonal and extremely halotolerant yeast. BMC
668 Genomics 19: 364. https://doi.org/10.1186/s12864-018-4751-5
669 Hu G. G., I. Liu, A. Sham, J. E. Stajich, F. S. Dietrich, *et al.*, 2008 Comparative hybridization
670 reveals extensive genome variation in the AIDS-associated pathogen Cryptococcus
671 neoformans. Genome Biol. 9: 17. https://doi.org/10.1186/gb-2008-9-2-r41
672 Hum Y. F., and S. Jinks-Robertson, 2019 Mismatch recognition and subsequent processing
673 have distinct effects on mitotic recombination intermediates and outcomes in yeast.
674 Nucleic Acids Research 47: 4554–4568. https://doi.org/10.1093/nar/gkz126
675 James T. Y., L. A. Michelotti, A. D. Glasco, R. A. Clemons, R. A. Powers, *et al.*, 2019
676 Adaptation by Loss of Heterozygosity in Saccharomyces cerevisiae Clones Under
677 Divergent Selection. Genetics 213: 665–683.
678 https://doi.org/10.1534/genetics.119.302411
679 Janbon G., K. L. Ormerod, D. Paulet, E. J. Byrnes, V. Yadav, *et al.*, 2014 Analysis of the
680 genome and transcriptome of Cryptococcus neoformans var. grubii reveals complex
681 RNA expression and microevolution leading to virulence attenuation. PLoS Genet 10:
682 e1004261. https://doi.org/10.1371/journal.pgen.1004261

683 Kavanaugh L. A., J. A. Fraser, and F. S. Dietrich, 2006 Recent evolution of the human pathogen
684 Cryptococcus neoformans by intervarietal transfer of a 14-gene fragment. Mol. Biol.
685 Evol. 23: 1879–1890. https://doi.org/10.1093/molbev/msl070
686 Lengeler K. B., G. M. Cox, and J. Heitman, 2001 Serotype AD strains of Cryptococcus
687 neoformans are diploid or aneuploid and are heterozygous at the mating-type locus.
688 Infect. Immun. 69: 115–122.
689 Li H., and R. Durbin, 2009 Fast and accurate short read alignment with Burrows-Wheeler
690 transform. Bioinformatics 25: 1754–1760. https://doi.org/10.1093/bioinformatics/btp324
691 Li H., B. Handsaker, A. Wysoker, T. Fennell, J. Ruan, *et al.*, 2009 The Sequence
692 Alignment/Map format and SAMtools. Bioinformatics 25: 2078–2079.
693 https://doi.org/10.1093/bioinformatics/btp352
694 Li W. J., A. F. Averette, M. Desnos-Ollivier, M. Ni, F. Dromer, *et al.*, 2012 Genetic diversity and
695 genomic plasticity of Cryptococcus neoformans AD hybrid strains. G3-Genes Genomes
696 Genetics 2: 83–97. https://doi.org/10.1534/g3.111.001255
697 Lin X. R., K. Nielsen, S. Patel, and J. Heitman, 2008 Impact of mating type, serotype, and ploidy
698 on the virulence of Cryptococcus neoformans. Infect. Immun. 76: 2923–2938.
699 https://doi.org/10.1128/iai.00168-08
700 Litvintseva A. P., X. Lin, I. Templeton, J. Heitman, and T. G. Mitchell, 2007 Many globally
701 isolated AD hybrid strains of Cryptococcus neoformans originated in Africa. PLoS
702 Pathog. 3: 1109–1117. https://doi.org/10.1371/journal.ppat.0030114
703 Loftus B. J., E. Fung, P. Roncaglia, D. Rowley, P. Amedeo, *et al.*, 2005 The genome of the
704 basidiomycetous yeast and human pathogen Cryptococcus neoformans. Science 307:
705 1321–1324. https://doi.org/10.1126/science.1103773
706 Mallet J., 2007 Hybrid speciation. Nature 446: 279–283. https://doi.org/10.1038/nature05706

Marcet-Houben M., and T. Gabaldón, 2015 Beyond the whole-genome duplication: Phylogenetic evidence for an ancient interspecies hybridization in the baker's yeast lineage. PLOS Biology 13: e1002220. https://doi.org/10.1371/journal.pbio.1002220

McKenna A., M. Hanna, E. Banks, A. Sivachenko, K. Cibulskis, *et al.*, 2010 The Genome Analysis Toolkit: A MapReduce framework for analyzing next-generation DNA sequencing data. Genome Res. 20: 1297–1303. https://doi.org/10.1101/gr.107524.110

Mixão V., and T. Gabaldón, 2020 Genomic evidence for a hybrid origin of the yeast opportunistic pathogen Candida albicans. BMC Biology 18: 48. https://doi.org/10.1186/s12915-020-00776-6

Opperman R., E. Emmanuel, and A. A. Levy, 2004 The effect of sequence divergence on recombination between direct repeats in Arabidopsis. Genetics 168: 2207–2215. https://doi.org/10.1534/genetics.104.032896

Orr H. A., and M. Turelli, 2001 The evolution of postzygotic isolation: accumulating Dobzhansky-Muller incompatibilities. Evolution 55: 1085–1094. https://doi.org/10.1111/j.0014-3820.2001.tb00628.x

Park H.-S., E. W. L. Chow, C. Fu, E. J. Soderblom, M. A. Moseley, *et al.*, 2016 Calcineurin targets involved in stress survival and fungal virulence. PLOS Pathogens 12: e1005873. https://doi.org/10.1371/journal.ppat.1005873

Phadke S. S., C. J. Maclean, S. Y. Zhao, E. A. Mueller, L. A. Michelotti, *et al.*, 2018 Genome-wide screen for Saccharomyces cerevisiae genes contributing to opportunistic pathogenicity in an invertebrate model host. G3-Genes Genomes Genetics 8: 63–78. https://doi.org/10.1534/g3.117.300245

Priest S. J., M. A. Coelho, V. Mixão, S. A. Clancey, Y. Xu, *et al.*, 2021 Factors enforcing the species boundary between the human pathogens Cryptococcus neoformans and Cryptococcus deneoformans. PLoS Genet 17: e1008871. https://doi.org/10.1371/journal.pgen.1008871

Pryszcz L. P., T. Németh, E. Saus, E. Ksiezopolska, E. Hegedüsová, *et al.*, 2015 The genomic aftermath of hybridization in the opportunistic pathogen Candida metapsilosis. Plos Genetics 11: e1005626. https://doi.org/10.1371/journal.pgen.1005626

Quinlan A. R., and I. M. Hall, 2010 BEDTools: a flexible suite of utilities for comparing genomic features. Bioinformatics 26: 841–842. https://doi.org/10.1093/bioinformatics/btq033

R_Core_Team, 2019 *R: A language and environment for statistical computing*. R Foundation for Statistical Computing, Vienna, Austria. URL: http://www.R-project.org/.

Rhodes J., C. A. Desjardins, S. M. Sykes, M. A. Beale, M. Vanhove, *et al.*, 2017 Tracing genetic exchange and biogeography of Cryptococcus neoformans var. grubii at the global population level. Genetics 207: 327–346. https://doi.org/10.1534/genetics.117.203836

Rieseberg L. H., M. A. Archer, and R. K. Wayne, 1999 Transgressive segregation, adaptation and speciation. Heredity 83: 363–372. https://doi.org/10.1038/sj.hdy.6886170

Rieseberg L. H., 2001 Polyploid evolution: Keeping the peace at genomic reunions. Current Biology 11: R925–R928. https://doi.org/10.1016/S0960-9822(01)00556-5

Roth C., S. Sun, R. B. Billmyre, J. Heitman, and P. M. Magwene, 2018 A high-resolution map of meiotic recombination in Cryptococcus deneoformans demonstrates decreased recombination in unisexual reproduction. Genetics 209: 567–578. https://doi.org/10.1534/genetics.118.300996

Saikkonen K., C. A. Young, M. Helander, and C. L. Schardl, 2016 Endophytic Epichloë species and their grass hosts: from evolution to applications. Plant Mol. Biol. 90: 665–675. https://doi.org/10.1007/s11103-015-0399-6

Samarasinghe H., and J. Xu, 2018 Hybrids and hybridization in the Cryptococcus neoformans and Cryptococcus gattii species complexes. Infect. Genet. Evol. 66: 245–255. https://doi.org/10.1016/j.meegid.2018.10.011

757 Samarasinghe H., M. You, T. S. Jenkinson, J. Xu, and T. Y. James, 2020a Hybridization
758 facilitates adaptive evolution in two major fungal pathogens. Genes (Basel) 11: 101.
759 https://doi.org/10.3390/genes11010101
760 Samarasinghe H., A. Vogan, N. Pum, and J. Xu, 2020b Patterns of allele distribution in a hybrid
761 population of the Cryptococcus neoformans species complex. Mycoses 63: 275–283.
762 https://doi.org/10.1111/myc.13040
763 Schardl C. L., and K. D. Craven, 2003 Interspecific hybridization in plant-associated fungi and
764 oomycetes: a review. Mol. Ecol. 12: 2861–2873. https://doi.org/10.1046/j.1365-
765 294X.2003.01965.x
766 Schröder M. S., K. M. de S. Vicente, T. H. R. Prandini, S. Hammel, D. G. Higgins, *et al.*, 2016
767 Multiple origins of the pathogenic yeast Candida orthopsilosis by separate hybridizations
768 between two parental species. PLOS Genetics 12: e1006404.
769 https://doi.org/10.1371/journal.pgen.1006404
770 Seplyarskiy V. B., M. D. Logacheva, A. A. Penin, M. A. Baranova, E. V. Leushkin, *et al.*, 2014
771 Crossing-over in a hypervariable species preferentially occurs in regions of high local
772 smilarity. Molecular Biology and Evolution 31: 3016–3025.
773 https://doi.org/10.1093/molbev/msu242
774 Shapira R., T. Levy, S. Shaked, E. Fridman, and L. David, 2014 Extensive heterosis in growth of
775 yeast hybrids is explained by a combination of genetic models. Heredity 113: 316–326.
776 https://doi.org/10.1038/hdy.2014.33
777 St Charles J., E. Hazkani-Covo, Y. Yin, S. L. Andersen, F. S. Dietrich, *et al.*, 2012 High-
778 resolution genome-wide analysis of irradiated (UV and gamma-rays) diploid yeast cells
779 reveals a high frequency of genomic loss of heterozygosity (LOH) events. Genetics 190:
780 1267–1284. https://doi.org/10.1534/genetics.111.137927

781 Steenwyk J. L., A. L. Lind, L. N. A. Ries, T. F. dos Reis, L. P. Silva, *et al.*, 2020 Pathogenic
782 allodiploid hybrids of Aspergillus fungi. Current Biology 30: 2495-2507.e7.
783 https://doi.org/10.1016/j.cub.2020.04.071
784 Stone N. R. H., J. Rhodes, M. C. Fisher, S. Mfinanga, S. Kivuyo, *et al.*, 2019 Dynamic ploidy
785 changes drive fluconazole resistance in human cryptococcal meningitis. J Clin Invest
786 129: 999–1014. https://doi.org/10.1172/JCI124516
787 Stukenbrock E. H., 2016 The role of hybridization in the evolution and emergence of new fungal
788 plant pathogens. Phytopathology 106: 104–112. https://doi.org/10.1094/phyto-08-15-
789 0184-rvw
790 Sui Y., L. Qi, J.-K. Wu, X.-P. Wen, X.-X. Tang, *et al.*, 2020 Genome-wide mapping of
791 spontaneous genetic alterations in diploid yeast cells. PNAS 117: 28191–28200.
792 https://doi.org/10.1073/pnas.2018633117
793 Sun S., and J. P. Xu, 2007 Genetic analyses of a hybrid cross between serotypes A and D
794 strains of the human pathogenic fungus Cryptococcus neoformans. Genetics 177: 1475–
795 1486. https://doi.org/10.1534/genetics.107.078923
796 Sun S., and J. Xu, 2009 Chromosomal rearrangements between serotype A and D strains in
797 Cryptococcus neoformans. PLoS ONE 4: e5524.
798 Sun S., R. B. Billmyre, P. A. Mieczkowski, and J. Heitman, 2014 Unisexual reproduction drives
799 meiotic recombination and phenotypic and karyotypic plasticity in Cryptococcus
800 neoformans. PLOS Genetics 10: e1004849.
801 https://doi.org/10.1371/journal.pgen.1004849
802 Symington L. S., R. Rothstein, and M. Lisby, 2014 Mechanisms and regulation of mitotic
803 recombination in Saccharomyces cerevisiae. Genetics 198: 795–835.
804 https://doi.org/10.1534/genetics.114.166140

805 Tattini L., N. Tellini, S. Mozzachiodi, M. D'Angiolo, S. Loeillet, *et al.*, 2019 Accurate tracking of
806 the mutational landscape of diploid hybrid genomes. Molecular Biology and Evolution 36:
807 2861–2877. https://doi.org/10.1093/molbev/msz177
808 Treangen T. J., B. D. Ondov, S. Koren, and A. M. Phillippy, 2014 The Harvest suite for rapid
809 core-genome alignment and visualization of thousands of intraspecific microbial
810 genomes. Genome Biology 15: 524. https://doi.org/10.1186/s13059-014-0524-x
811 Vogan A. A., J. Khankhet, and J. Xu, 2013 Evidence for mitotic recombination within the basidia
812 of a hybrid cross of Cryptococcus neoformans. PLoS ONE 8: e62790.
813 https://doi.org/10.1371/journal.pone.0062790
814 Vogan A. A., and J. Xu, 2014 Evidence for genetic incompatibilities associated with post-zygotic
815 reproductive isolation in the human fungal pathogen Cryptococcus neoformans. Genome
816 57: 335–344. https://doi.org/10.1139/gen-2014-0077
817 Vogan A. A., J. Khankhet, H. Samarasinghe, and J. P. Xu, 2016 Identification of QTLs
818 associated with virulence related traits and drug resistance in Cryptococcus neoformans.
819 G3-Genes Genomes Genet. 6: 2745–2759. https://doi.org/10.1534/g3.116.029595
820 Wickham H., 2009 *ggplot2: Elegant Graphics for Data Analysis*. Springer-Verlag, New York.
821 Xu J., A. R. Ramos, R. Vilgalys, and T. G. Mitchell, 2000a Clonal and spontaneous origins of
822 fluconazole resistance in Candida albicans. J Clin Microbiol 38: 1214–1220.
823 https://doi.org/10.1128/JCM.38.3.1214-1220.2000
824 Xu J., R. Vilgalys, and T. G. Mitchell, 2000b Multiple gene genealogies reveal recent dispersion
825 and hybridization in the human pathogenic fungus Cryptococcus neoformans. Mol. Ecol.
826 9: 1471–1481. https://doi.org/10.1046/j.1365-294x.2000.01021.x
827 Xu J. P., G. Z. Luo, R. J. Vilgalys, M. E. Brandt, and T. G. Mitchell, 2002 Multiple origins of
828 hybrid strains of Cryptococcus neoformans with serotype AD. Microbiology-(UK) 148:
829 203–212.

830 Yu G., L.-G. Wang, Y. Han, and Q.-Y. He, 2012 clusterProfiler: an R package for comparing
831 biological themes among gene clusters. OMICS 16: 284–287.
832 https://doi.org/10.1089/omi.2011.0118
833
834 Figure legends
835
836 **Figure 1**. Clones evolved in *in vitro* conditions mostly showed fitness gains regardless of means
837 of estimation. Shown are values of relative fitness comparing a clone grown in the same media
838 in which evolution occurred relative to the fitness of the ancestral genotype SSD-719 (dashed
839 line). A) Fitness measured using doubling time. B) Fitness measured using EOG = Efficiency of
840 Growth (i.e., carrying capacity). C) Fitness measured using relative competitive growth in the
841 presence of a marked ancestral strain. Each dot represents an individual clone. Boxes indicate
842 the 25-75% percentiles, bars indicate medians, and the whiskers extend to 1.5 x the
843 interquartile range. Cana=minimal media with a sublethal concentration of canavanine (2 mg/L)
844 plus arginine (4 mg/L), and NaCl=complete media with 1.0 M NaCl. Wine strains were not
845 tested by growth curve analysis due to opacity of the medium which prevented accurate
846 readings by spectrophotometry.
847
848 **Figure 2**. Strains passaged in larvae showed overall greater fitness than the ancestor as
849 measured by recovery after 2 days growth post-coinjection with a common competitor strain
850 (SSE-761). Three replicate experiments were conducted for each strain, and values indicate
851 mean (+1 sd). All values are shown relative to the fitness of SSD-719 (ancestor) which was set
852 to 1.0. Post-Hoc comparisons of the fitness between each evolved strain and the ancestor by
853 Fisher's Least Significant Difference test found only the difference between SSD-719 and
854 P5W10 to be significant (P=0.0039). P4W10 and P6W10 were significantly different from SSD-
855 719 to a lesser degree (P=0.06 and P=0.07, respectively).

856

857 **Figure 3**. Landscape of LOH across the 14 chromosomes of the evolved clones. Shown are
858 genotypes at 10 kb resolution of the strains, with media type shown on the left margin and strain
859 name on the right margin. The ancestral genotype of the *in vivo* (larval) passaging was different
860 from the *in vitro* (other media types), because the experiments began at different times. The
861 reference genome coordinates are from the *C. neoformans* parent. White regions represent
862 unmapped, typically repetitive regions of the genome, or regions of the genome that had
863 undergone LOH in the ancestral diploid strains. In particular, ~260 kb of the right arm of Chr. 2
864 underwent an LOH event in the ancestor before passaging.

865

866 **Figure 4.** Summary of detected LOH mechanisms across the 35 evolved hybrid clones. (A) A
867 depiction of proposed LOH mechanisms according to schema defined by St. Charles (St
868 Charles *et al.* 2012), and (B) Tallied numbers of events observed among the hybrid clones.
869 **Figure 5.** Mapping of reads to a hybrid reference genome of strains evolved in canavanine
870 reveals trisomies and whole chromosome LOH. Bars show mean depth in 5 kb intervals that
871 have been normalized by dividing the depth of each interval by the mean coverage for each
872 strain. For each strain the top panel shows mapping to the *C. neoformans* reference genome,
873 and the bottom panel shows mapping to the *C. deneoformans* reference genome. Diagrams of
874 homeologous chromosomes are shown above each reference genome where colors reflect
875 homology and black stripes indicate centromeres. *C. deneoformans* chromosomes were
876 rearranged to better reflect homology, and asterisks indicate chromosomes that have been
877 reverse-complemented. Black arrows in strain CC-100-1 indicate loss of the *C. neoformans* Chr.
878 4 copy and gain of the homeologous *C. deneoformans* Chr. 12 copy, likely indicating LOH
879 ongoing during the growth of the strain for DNA extraction. Red arrow in CC-100-5 indicates a
880 region of the left arm of *C. deneoformans* Chr. 13 that had undergone apparent deletion.

881

882 **Figure 6.** Chromosome composition of the 35 evolved clones and the ancestors reveals at least
883 one trisomy in most strains. Partial aneuploidies are indicated as partial chromosomes that are
884 not shown to scale. Shaded boxes indicate partial or complete aneuploidy for *C. neoformans*
885 (red) or *C. deneoformans* (blue) homeologues. Recombined chromosomes are not indicated
886 with the exception of a few chromosomes with larger exchanges. Footnotes indicate strains
887 which had evidence for mixed genotype composition; all notes refer to *C. neoformans*
888 chromosome numbers. 1. SSD719-in vivo and P6W10 showed a pattern consistent with a
889 mixed population of trisomies for *C. neoformans* or *C. deneoformans* Chr. 6. 2. Strain CW-100-4
890 has a pattern consistent with either an equal mixture of two strains with different aneuploidies or
891 a strain that is largely tetraploid. 3. Strain CN-100-2 has a pattern consistent with *C. neoformans*
892 Chr. 12 apparently present in small subpopulation. 4. CC-100-1 has a pattern of apparent active
893 loss of *C. neoformans* Chr. 4 and duplication of the corresponding homeologue *C.*
894 *deneoformans* Chr. 12 (arrow in **Figure 5**). For additional details on the mapping see depth of
895 coverage plots (**Figure 5**; **Suppl. Figures 1-6**).
896
897 **Figure 7**. Locations of mitotic recombination breakpoints are non-random across the genome.
898 Blue dots indicate the average heterozygosity in 10 kb windows between *C. neoformans* and *C.*
899 *deneoformans* parental genomes that passed our filtering strategies. Green boxes indicate
900 locations of LOH events, and when accompanied by dark grey bars they indicate longer LOH
901 tracts.

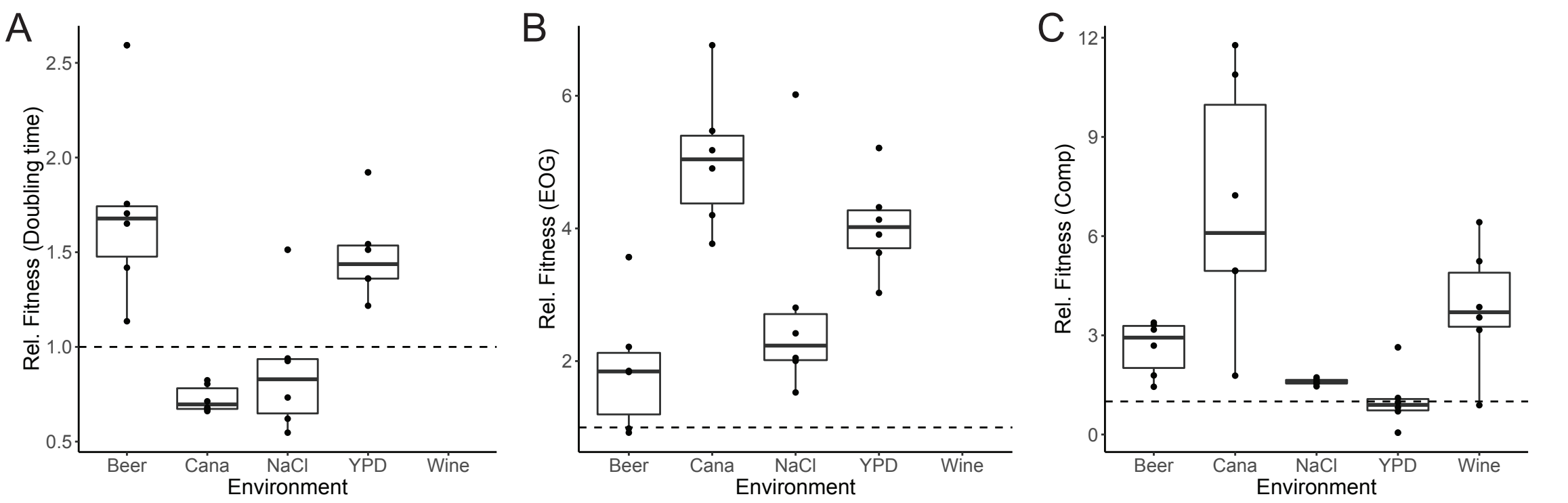
A
Rel. Fitness (Doubling time)
2.5
2.0
1.5
1.0
0.5
Beer
Cana
NaCl
YPD
Wine
Environment
B
Rel. Fitness (EOG)
6
4
2
Beer
Cana
NaCl
YPD
Wine
Environment
C
Rel. Fitness (Comp)
12
9
6
3
0
Beer
Cana
NaCl
YPD
Wine
Environment

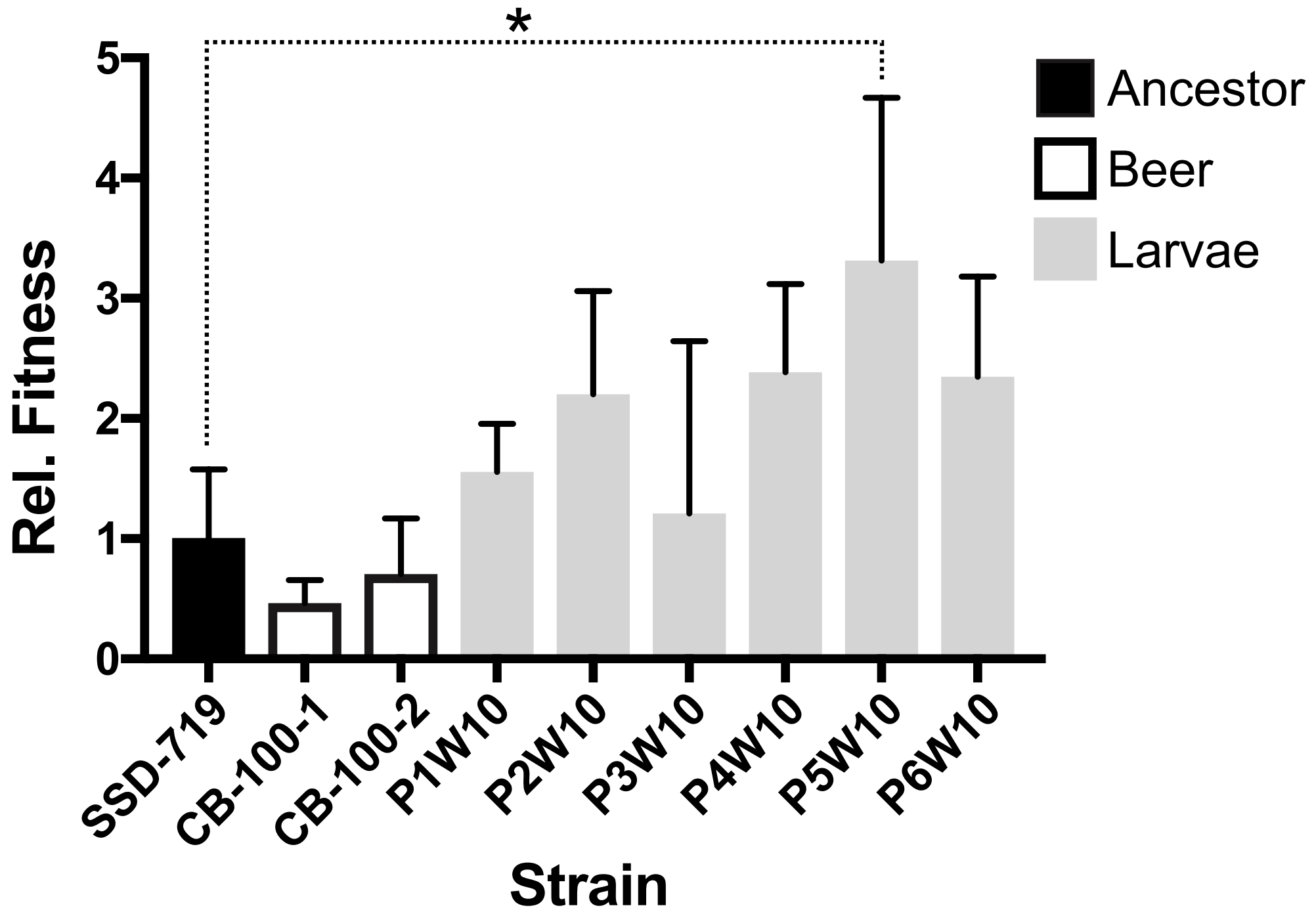
*
Ancestor
Beer
Larvae
Rel. Fitness
0
1
2
3
4
5
SSD-719
CB-100-1
CB-100-2
P1W10
P2W10
P3W10
P4W10
P5W10
P6W10
Strain

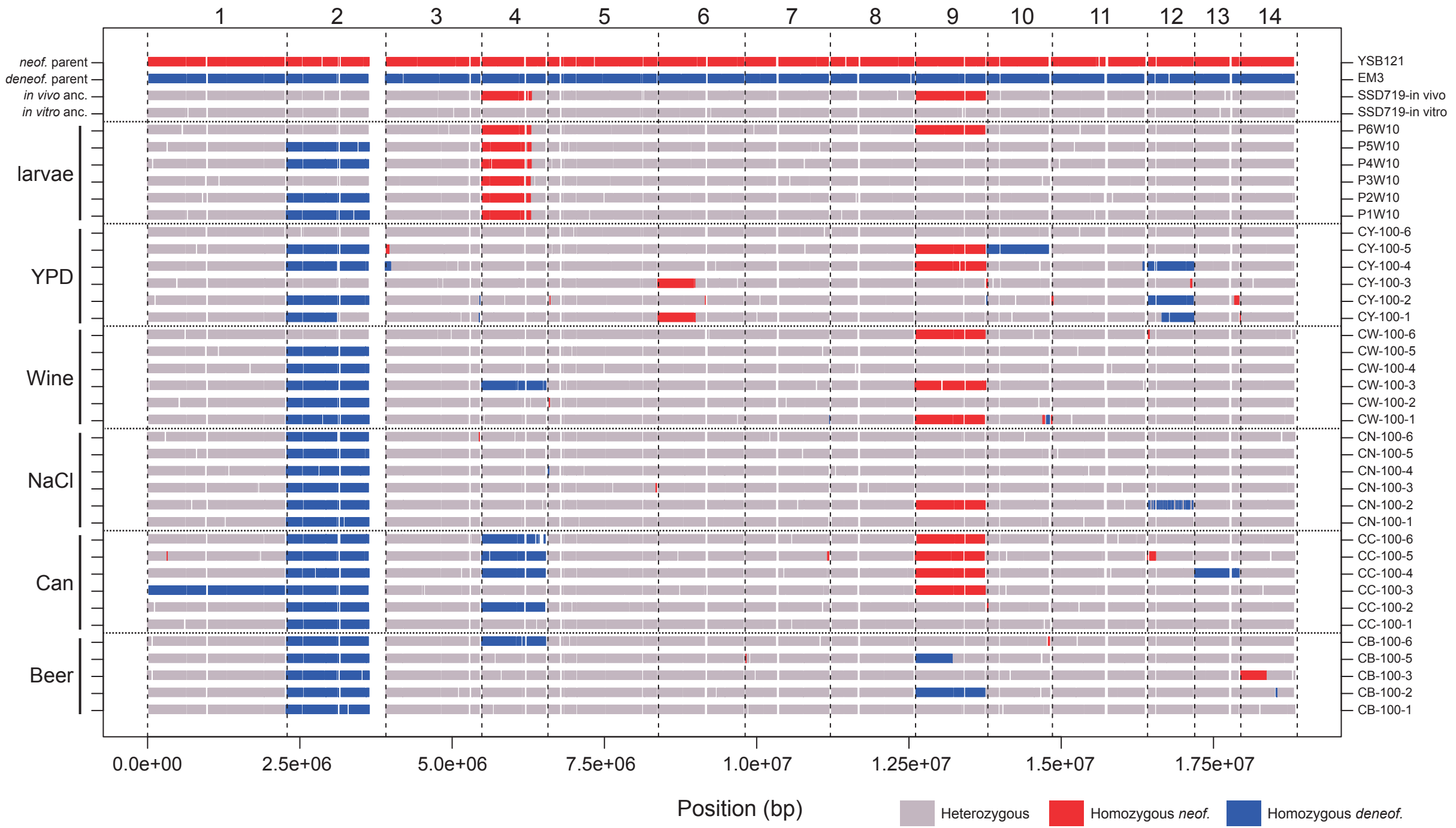
1
2
3
4
5
6
7
8
9
10
11
12
13
14
neof. parent
deneof. parent
in vivo anc.
in vitro anc.
larvae
YPD
Wine
NaCl
Can
Beer
YSB121
EM3
SSD719-in vivo
SSD719-in vitro
P6W10
P5W10
P4W10
P3W10
P2W10
P1W10
CY-100-6
CY-100-5
CY-100-4
CY-100-3
CY-100-2
CY-100-1
CW-100-6
CW-100-5
CW-100-4
CW-100-3
CW-100-2
CW-100-1
CN-100-6
CN-100-5
CN-100-4
CN-100-3
CN-100-2
CN-100-1
CC-100-6
CC-100-5
CC-100-4
CC-100-3
CC-100-2
CC-100-1
CB-100-6
CB-100-5
CB-100-3
CB-100-2
CB-100-1
0.0e+00
2.5e+06
5.0e+06
7.5e+06
1.0e+07
1.25e+07
1.5e+07
1.75e+07
Position (bp)
Heterozygous
Homozygous neof.
Homozygous deneof.

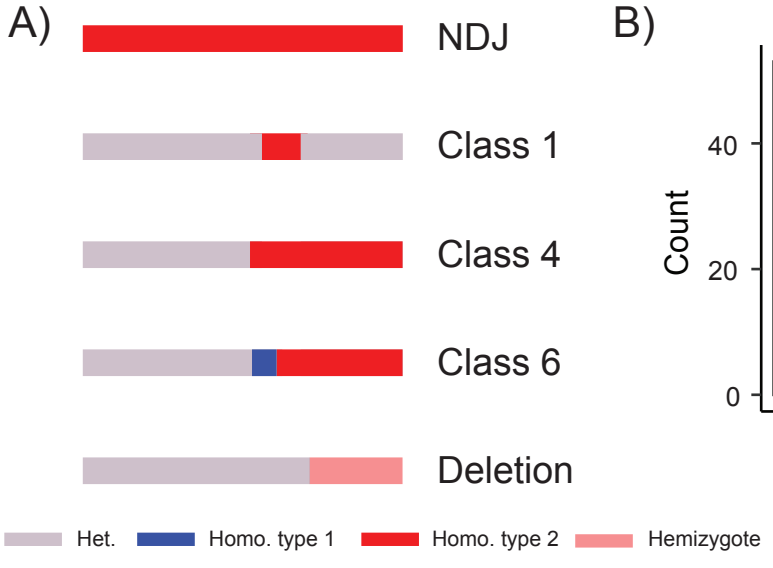
A)
NDJ
Class 1
Class 4
Class 6
Deletion
B)
Count
40
20
0
NDJ
1
4
6
Deletion
Mechanism
Het.
Homo. type 1
Homo. type 2
Hemizygote

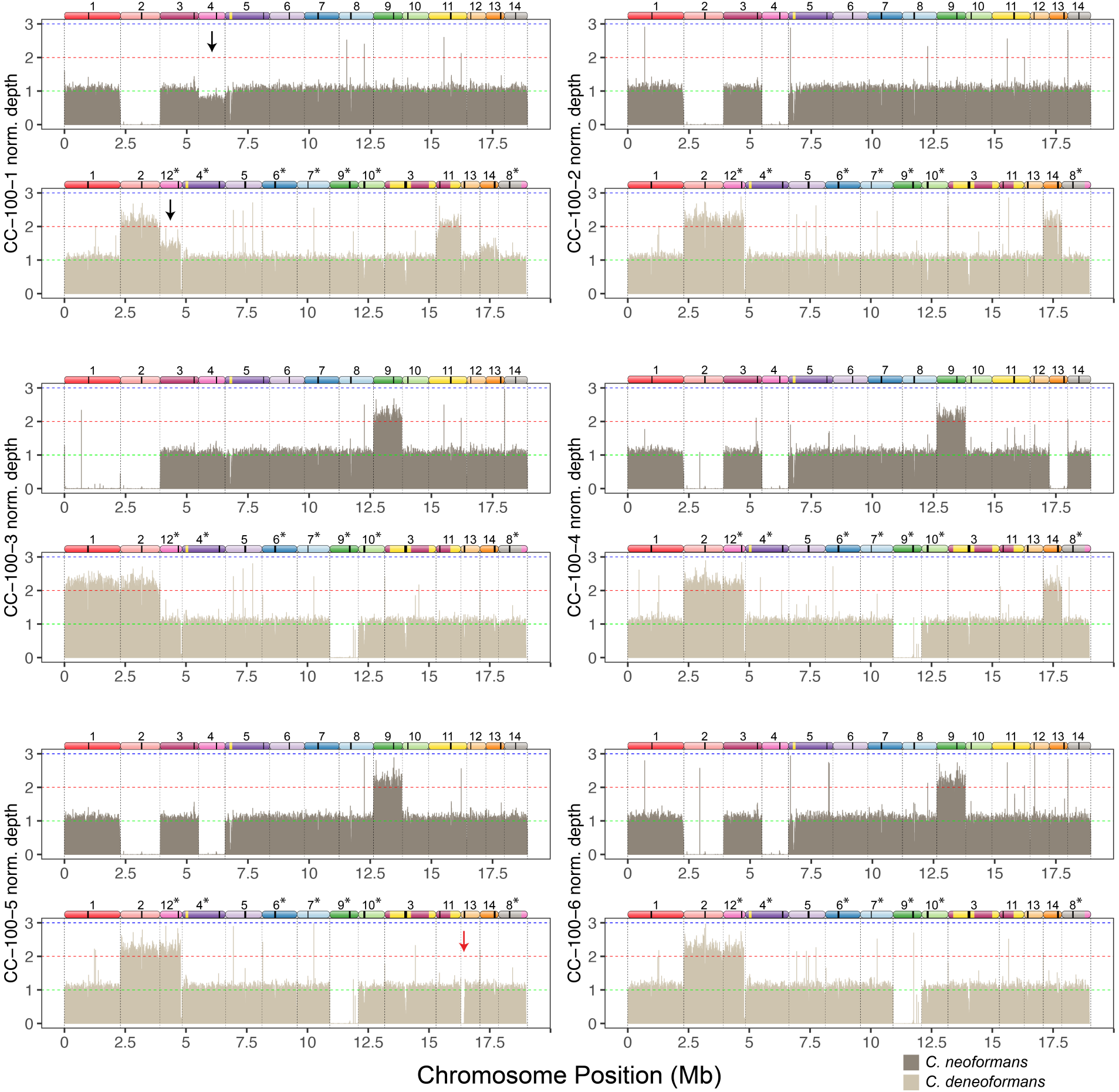
CC−100−1 norm. depth
CC−100−2 norm. depth
CC−100−3 norm. depth
CC−100−4 nrom. depth
CC−100−5 norm. depth
CC−100−6 norm. depth
Chromosome Position (Mb)
C. neoformans
C. deneoformans

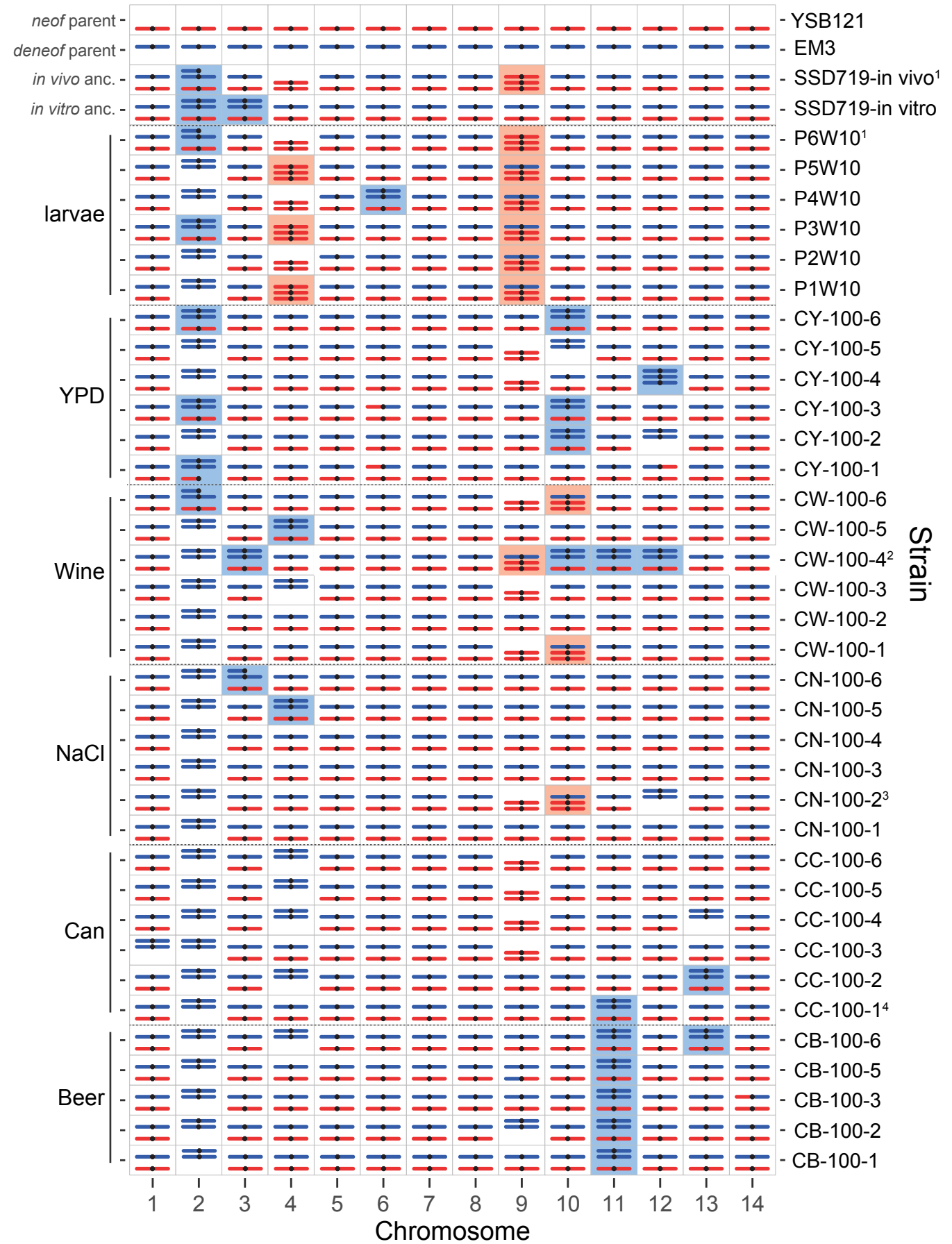
neof parent
deneof parent
in vivo anc.
in vitro anc.
larvae
YPD
Wine
NaCl
Can
Beer
YSB121
EM3
SSD719-in vivo1
SSD719-in vitro
P6W10[1]
P5W10
P4W10
P3W10
P2W10
P1W10
CY-100-6
CY-100-5
CY-100-4
CY-100-3
CY-100-2
CY-100-1
CW-100-6
CW-100-5
CW-100-4[2]
CW-100-3
CW-100-2
CW-100-1
CN-100-6
CN-100-5
CN-100-4
CN-100-3
CN-100-2[3]
CN-100-1
CC-100-6
CC-100-5
CC-100-4
CC-100-3
CC-100-2
CC-100-1[4]
CB-100-6
CB-100-5
CB-100-3
CB-100-2
CB-100-1
Strain
1
2
3
4
5
6
7
8
9
10
11
12
13
14
Chromosome

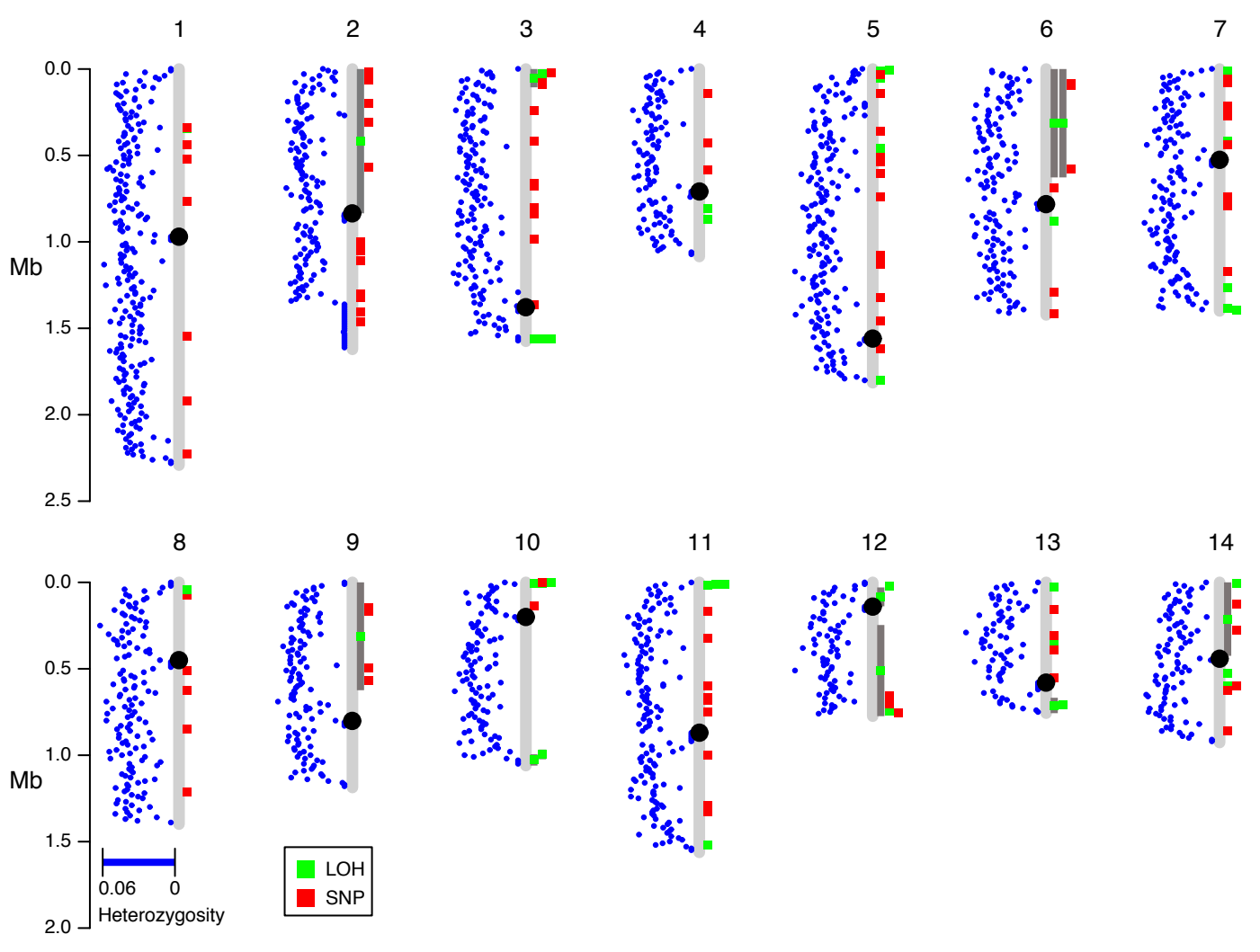
1
2
3
4
5
6
7
8
9
10
11
12
13
14
0.0
0.5
1.0
1.5
2.0
2.5
Mb
0.06
0
Heterozygosity
LOH
SNP

Suppl. Table 1. Markers used for screening mating products for heterozygosity. Chromosome numbers and positions are relative to the H99 genome.

Marker	Chromosome	Position	Forward Primer (5' - 3')	Reverse Primer (5' - 3')
Chrom01_Region5	1	128800-131200	GCACATGAAGAAATATGACCG	GCACATTCGCCAATCCTATC
Chrom01_Region8	1	389600-391200	AATGAGACGAATACGGTCGG	AGCTCTCTTTCACTGACACGA
Chrom02_Region1	2	88000-89600	GCACAGGCCAGTAAAGGAGG	GAATCTGAGAAGGCTGAGGCTA
Chrom02_Region5	2	1228800-1231200	GCTGCTGCATTTGCTGAG	TGAAATGAACGAACTAGTACGG
Chrom07_Region1	7	56800-59200	CGCCCTCTTGCTGAAGTTG	TTTCTCTTGTGCTTCAAATGC
Chrom07_Region5	7	512800-514400	GAAATGGTGCGAGAATAGGC	CATCTGCACTTCGAACGAC
Chrom10_Region7	10	967200-968000	ATTTTCAGGTATCCCCATGC	CATTGGTAAACTCGCCTCTG
Chrom12_Region1	12	87200-88800	GGAACGAGATGGAAATCGG	GTCTCACTGCCAGTAAAGTCAG
Chrom12_Region8	12	721600-724000	GCCATTTGGACTTTGGGTG	TGACTCTTGTGGAGCTTAACG
Chrom13_Region1	13	108000-108800	CGCCTTTGATTGCTGATGAC	GGGATAGCTCTTGGCAATGC
Chrom13_Region4	13	693600-695200	GAAGCCATCTTGCTGAAGTG	TTCGGGAGGGTGACTCTC
STE20_neo_MATalpha	5	247512-247841	GGCTGCAATCACAGCACCTTAC	CTTCATGACATCACTCCCCTAT
STE20_deneo_MATa	5	n.a.	CACATCTCAGATGCCATTTTACCA	AGCTCTAAGTCATATGGGTTATAT

Suppl. Table 3. Heterozygosity across chromosomes is not correlated with frequency of crossover events or nondisjunction (NDJ). Data are relative to *C. neoformans* H99 genome. Only one breakpoint for each gene conversion is considered.

Chr	Size	Num SNPs	SNP rate	Num. breaks	NDJ
1	2291499	72959	0.0318	1	1
2	1621675	39814	0.0246	1	29
3	1575141	50117	0.0318	5	6
4	1084805	30247	0.0279	2	0
5	1814975	54199	0.0299	6	0
6	1422463	45598	0.0321	3	0
7	1399503	42668	0.0305	7	0
8	1398693	42582	0.0304	1	0
9	1186808	37586	0.0317	1	12
10	1059964	29439	0.0278	5	1
11	1561994	47038	0.0301	4	0
12	774062	20441	0.0264	4	3
13	756744	20401	0.0270	3	1
14	926563	27207	0.0294	4	0

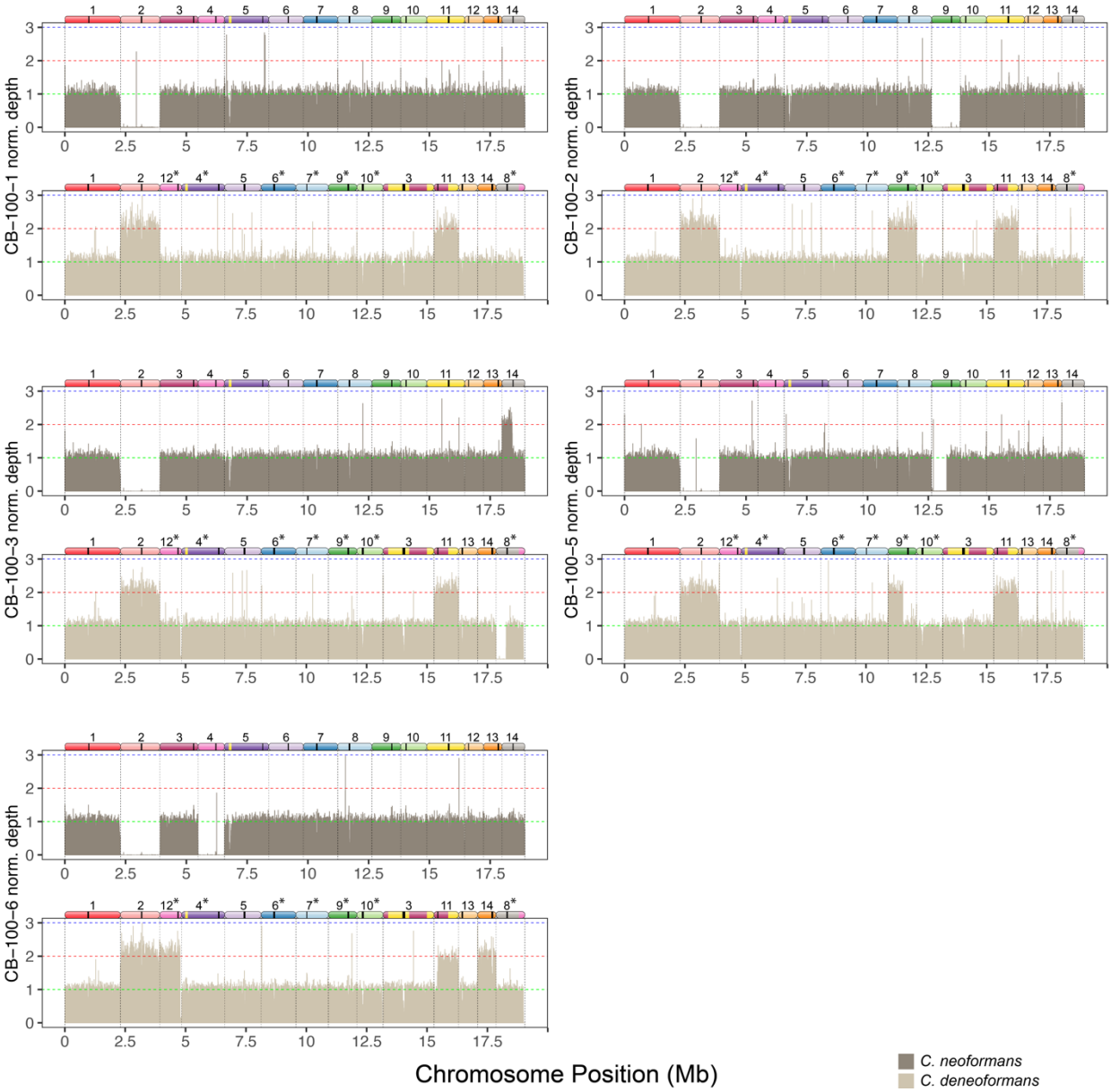

Suppl. Figure 1. Mapping of reads to a hybrid reference genome of strains evolved in beer wort. Bars show mean depth in 5 kb intervals that have been normalized by dividing the depth of each interval by the mean coverage for each strain. For each strain the top panel shows mapping to the *C. neoformans* reference genome, and the bottom panel shows mapping to the *C. deneoformans* reference genome. Diagrams of homeologous chromosomes are shown above each reference genome where colors reflect homology and black stripes indicate centromeres. *C. deneoformans* chromosomes were rearranged to better reflect homology, and asterisks indicate chromosomes that have been reverse-complemented.

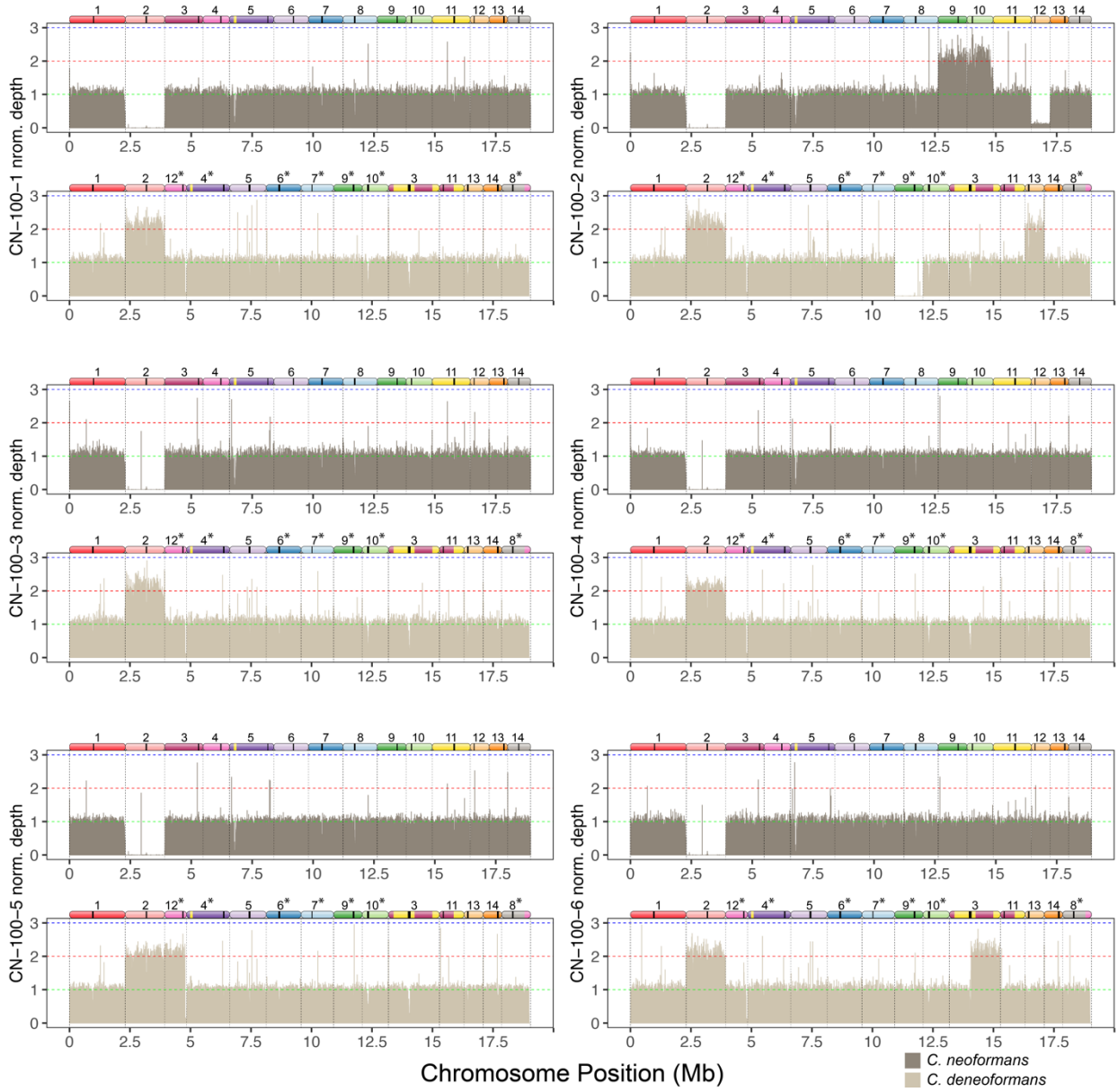

Suppl. Figure 2. Mapping of reads to a hybrid reference genome of strains evolved in high salt. Bars show mean depth in 5 kb intervals that have been normalized by dividing the depth of each interval by the mean coverage for each strain. For each strain the top panel shows mapping to the *C. neoformans* reference genome, and the bottom panel shows mapping to the *C. deneoformans* reference genome. Diagrams of homeologous chromosomes are shown above each reference genome where colors reflect homology and black stripes indicate centromeres. *C. deneoformans* chromosomes were rearranged to better reflect homology, and asterisks indicate chromosomes that have been reverse-complemented.

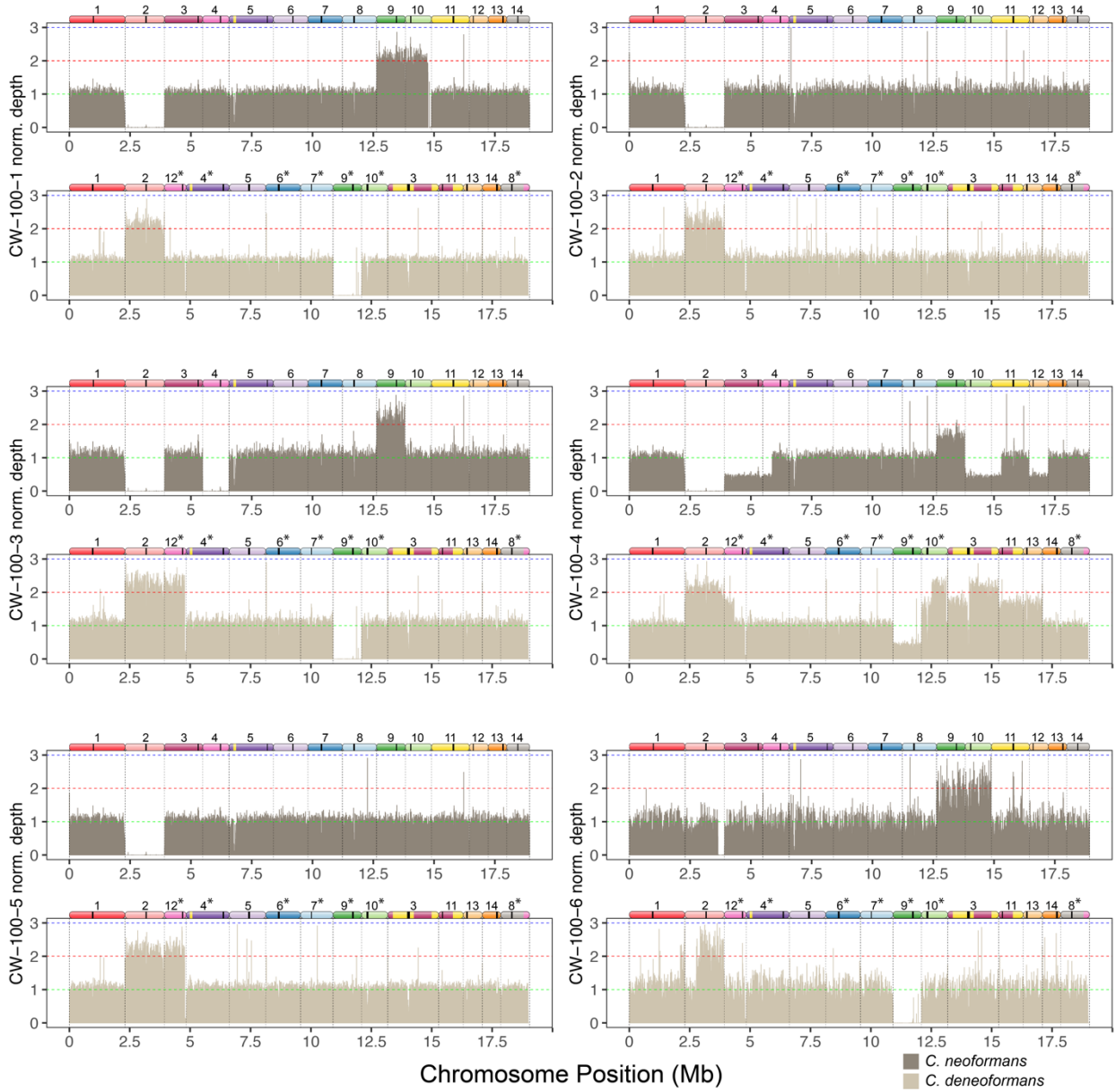

Suppl. Figure 3. Mapping of reads to a hybrid reference genome of strains evolved in wine must. Bars show mean depth in 5 kb intervals that have been normalized by dividing the depth of each interval by the mean coverage for each strain. For each strain the top panel shows mapping to the *C. neoformans* reference genome, and the bottom panel shows mapping to the *C. deneoformans* reference genome. Diagrams of homeologous chromosomes are shown above each reference genome where colors reflect homology and black stripes indicate centromeres. *C. deneoformans* chromosomes were rearranged to better reflect homology, and asterisks indicate chromosomes that have been reverse-complemented.

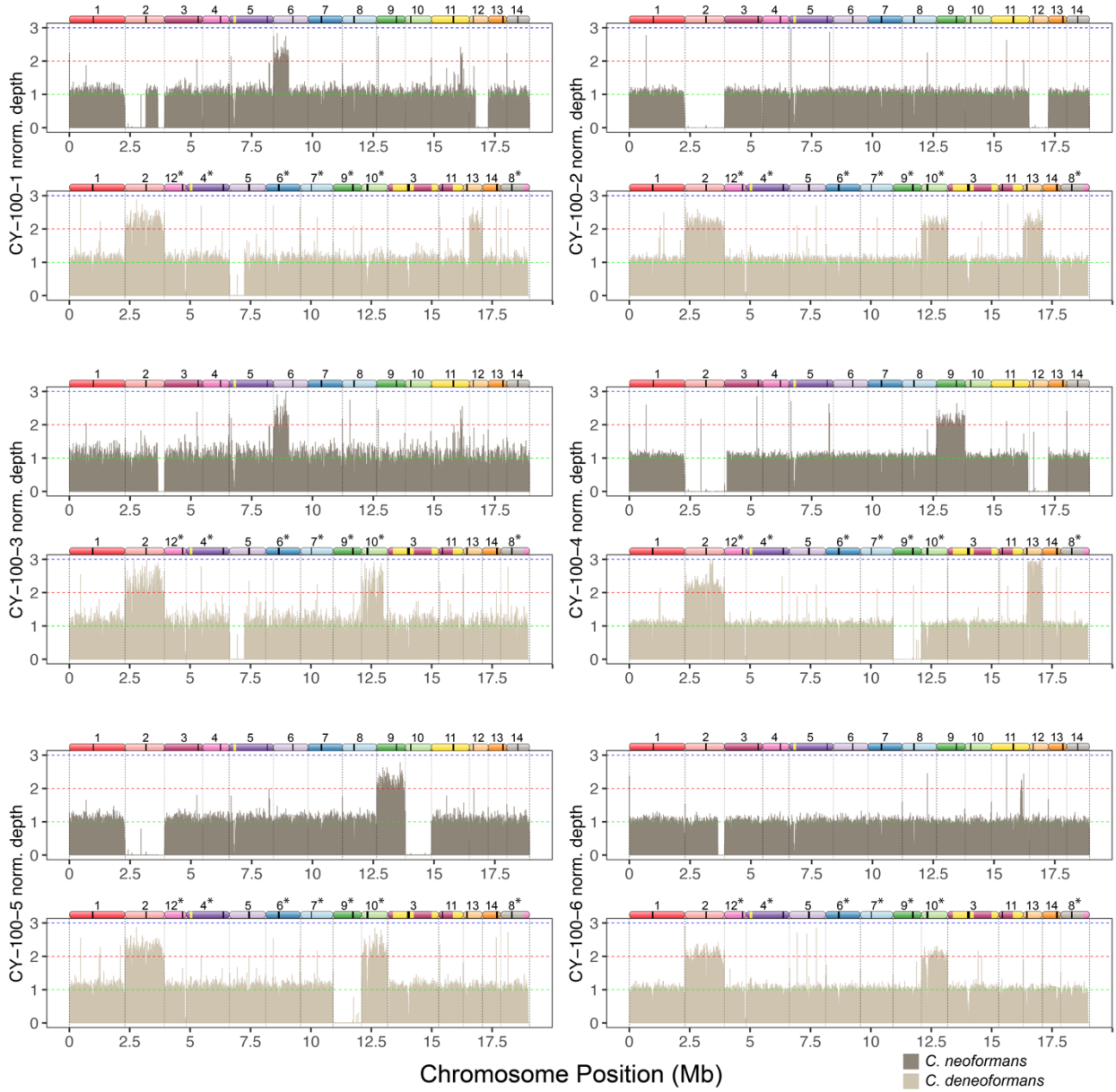

Suppl. Figure 4. Mapping of reads to a hybrid reference genome of strains evolved in complete media (YPD). Bars show mean depth in 5 kb intervals that have been normalized by dividing the depth of each interval by the mean coverage for each strain. For each strain the top panel shows mapping to the *C. neoformans* reference genome, and the bottom panel shows mapping to the *C. deneoformans* reference genome. Diagrams of homeologous chromosomes are shown above each reference genome where colors reflect homology and black stripes indicate centromeres. *C. deneoformans* chromosomes were rearranged to better reflect homology, and asterisks indicate chromosomes that have been reverse-complemented.

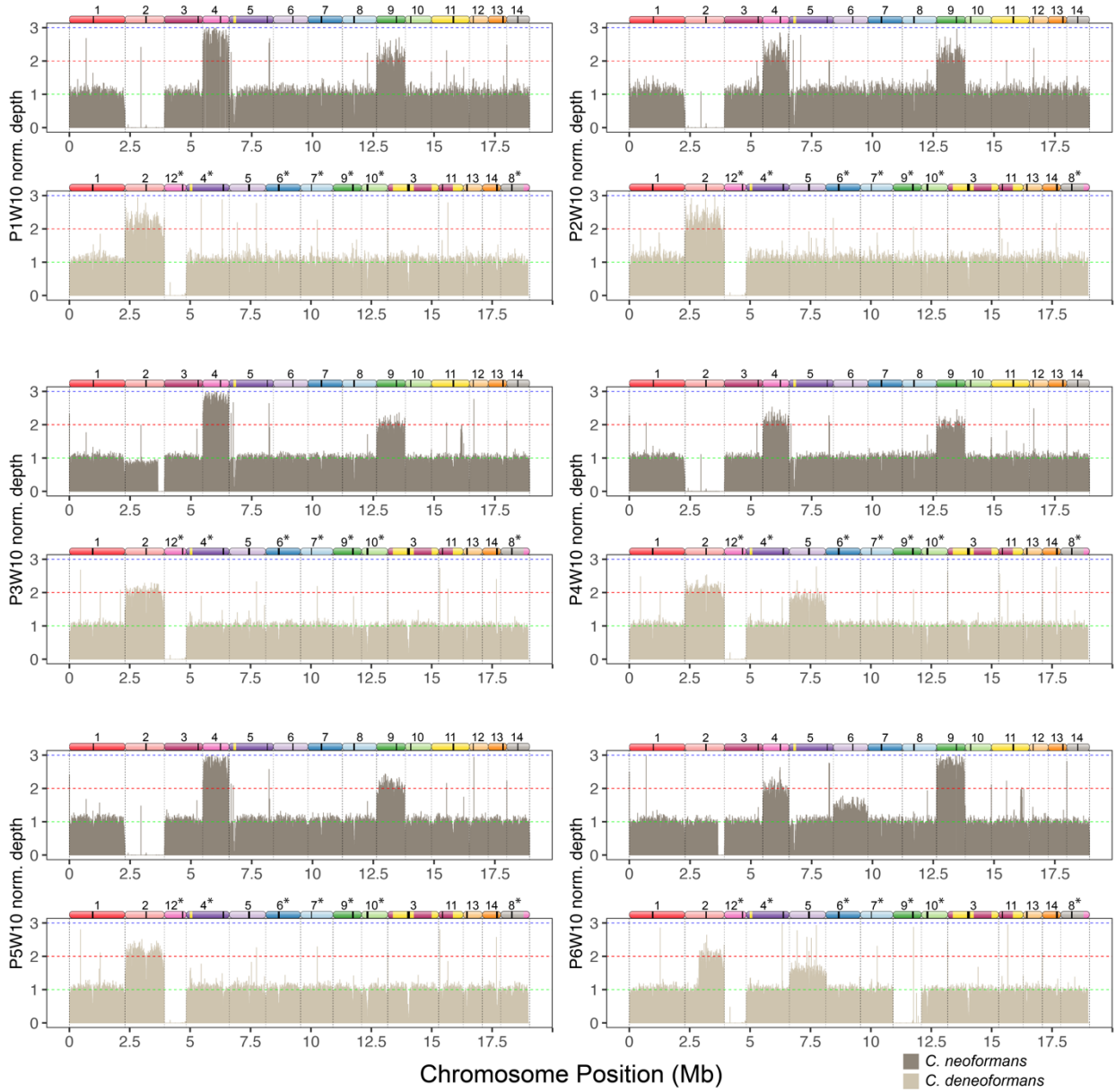

Suppl. Figure 5. Mapping of reads to a hybrid reference genome of strains evolved in larvae. Bars show mean depth in 5 kb intervals that have been normalized by dividing the depth of each interval by the mean coverage for each strain. For each strain the top panel shows mapping to the *C. neoformans* reference genome, and the bottom panel shows mapping to the *C. deneoformans* reference genome. Diagrams of homeologous chromosomes are shown above each reference genome where colors reflect homology and black stripes indicate centromeres. *C. deneoformans* chromosomes were rearranged to better reflect homology, and asterisks indicate chromosomes that have been reverse-complemented.

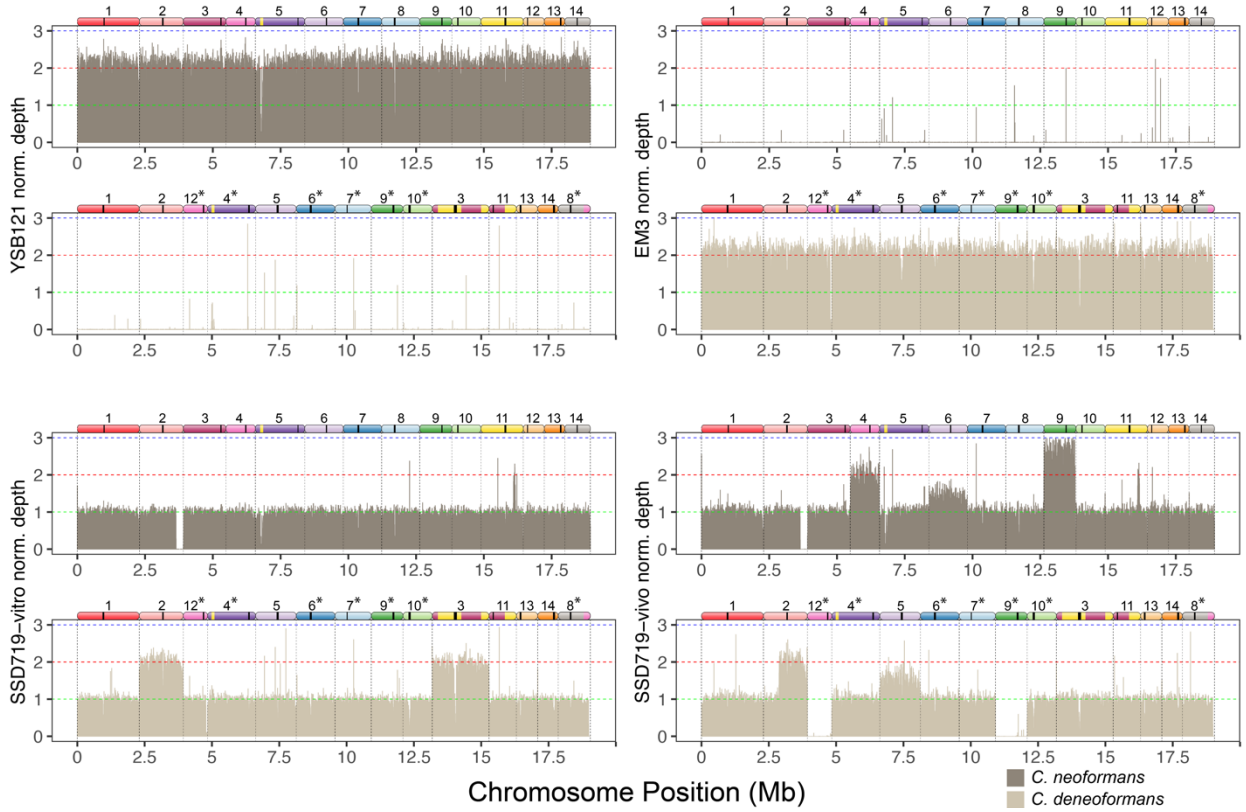

Suppl. Figure 6. Mapping of reads to a hybrid reference genome of ancestral strains. Strains YSB121 and EM3 are haploid *C. neoformans* and *C. deneoformans* parents, respectively. Strain SSD719-in vitro was used to initiate the in vitro evolution populations and strain SSD719-in vivo was used to initiate the passages in larvae. Bars show mean depth in 5 kb intervals that have been normalized by dividing the depth of each interval by the mean coverage for each strain. For each strain the top panel shows mapping to the *C. neoformans* reference genome, and the bottom panel shows mapping to the *C. deneoformans* reference genome. Diagrams of homeologous chromosomes are shown above each reference genome where colors reflect homology and black stripes indicate centromeres. *C. deneoformans* chromosomes were rearranged to better reflect homology, and asterisks indicate chromosomes that have been reverse-complemented.